CANADIAN THESES ON MICROFICHE

THÈSES CANADIENNES SUR MICROFICHE

National Library of Canada
Collections Development Branch

Canadian Theses on
Microfiche Service

Ottawa, Canada
K1A 0N4

Bibliothèque nationale du Canada
Direction du développement des collections

Service des thèses canadiennes
sur microfiche

NOTICE

The quality of this microfiche is heavily dependent upon the quality of the original thesis submitted for microfilming. Every effort has been made to ensure the highest quality of reproduction possible.

If pages are missing, contact the university which granted the degree.

Some pages may have indistinct print especially if the original pages were typed with a poor typewriter ribbon or if the university sent us an inferior photocopy.

Previously copyrighted materials (journal articles, published tests, etc.) are not filmed.

Reproduction in full or in part of this film is governed by the Canadian Copyright Act, R.S.C. 1970, c. C-30. Please read the authorization forms which accompany this thesis.

AVIS

La qualité de cette microfiche dépend grandement de la qualité de la thèse soumise au microfilmage. Nous avons tout fait pour, assurer une qualité supérieure de reproduction.

S'il manque des pages, veuillez communiquer avec l'université qui a conféré le grade.

La qualité d'impression de certaines pages peut laisser à désirer, surtout si les pages originales ont été dactylographiées à l'aide d'un ruban usé ou si l'université nous a fait parvenir une photocopie de qualité inférieure.

Les documents qui font déjà l'objet d'un droit d'auteur (articles de revue, examens publiés, etc.) ne sont pas microfilmés.

La reproduction, même partielle, de ce microfilm est soumise à la Loi canadienne sur le droit d'auteur, SRC 1970, c. C-30. Veuillez prendre connaissance des formules d'autorisation qui accompagnent cette thèse.

THIS DISSERTATION
HAS BEEN MICROFILMED
EXACTLY AS RECEIVED

LA THÈSE A ÉTÉ
MICROFILMÉE TELLE QUE
NOUS L'AVONS REÇUE

Canada

NL 339 (r. 85/09)

ANALYSIS OF AN OPEN-ENDED COAXIAL LINE SENSOR IN INHOMOGENEOUS DIELECTRICS

by

Lily S. Anderson

A thesis
presented to the University of Ottawa
in partial fulfillment of the
requirements for the degree of
Master of Applied Science
in
Department of Electrical Engineering

UNIVERSITÉ D'OTTAWA
UNIVERSITY OF OTTAWA

The University of Ottawa requires the signatures of all persons using or photocopying this thesis. Please sign below, and give address and date.

ABSTRACT

The capacitance of an open-ended coaxial line immersed in a bi-layered medium is evaluated both numerically and experimentally. Water layers of varying thickness backed by air and metal walls were assumed and a quasi-static solution for the fringe-field capacitance was obtained using the Method of Moments. The numerical results compared well with experimental values obtained using an automated network analyzer. The two configurations, namely the metal and air wall represent the upper and lower bound of the capacitance change from the homogeneous case, respectively. For a typical 6.4-mm (.25-in) diameter sensor, the change in the sensor capacitance as compared with a homogeneous case is less than 1% for layers thicker than 6 mm. The results of this investigation provide information on the response of the sensor when used to measure the properties of inhomogeneous dielectrics such as biological tissues.

ACKNOWLEDGMENTS

The author wishes to express her deepest gratitude to her supervisor Dr. S. S. Stuchly for his guidance and encouragement throughout this work. Thanks are also due to Dr. M. Ney for his valuable comments and discussions.

The author would also like to express her sincere thanks and appreciation to Mr. Gregory Gajda from the Communication Research Center, for his valuable suggestion, helpful advice, and encouragement throughout the course of this research and also for his comments on this thesis.

A heartfelt thanks is extended to all the staff members and graduate students of the Department of Electrical Engineering at the University of Ottawa, with whom the author had the priviledge of knowing, especially to Mr. G. Hartsgrove, Mr. S. Jhajharia, and Mr. S. Symons.

Finally, special thanks are due to my husband Ted for his encouragement and support during my studies.

GLOSSARY

List of symbols

a = inner conductor radius of the coaxial-line

b = outer conductor inner radius of the coaxial-line

c = outer conductor outer radius of the coaxial-line

C_T = static value of the total fringe-field capacitance

C_f = internal capacitance

C_o = external capacitance

C_{TEM} = capacitance due to the TEM field inside the line

d = position of the wall

E_r = electric field in r-component

E_z = electric field in z-component

E_T = magnitude of the total electric field intensity (resultant of the r-z components)

$E(k)$ = complete elliptic function of the first kind

$G(\hat{\varepsilon})$ = conductance

$G(s)$ = scalar potential Green's function

K = image coefficient

L = length of the coaxial-line

q = unit charge

S_{11} = magnitude of the input reflection coefficient

S_c = conductor surface

S_I = dielectric interface

V = potential difference

W_E = total stored electric energy

Y_o = characteristic admittance

Z_o = characteristic impedance

Greek

ψ = electric flux

ϕ = potential

ϕ = phase of the input reflection coefficient

$\hat{\epsilon}$ = permittivity of the medium

ϵ' = real part of the relative permittivity or dielectric constant

ϵ'' = loss factor of the medium corresponding to the imaginary part of $\hat{\epsilon}$

ϵ_0 = permittivity of free-space

ΔS_i = i-th subarea of the cylindrical coaxial-line

σ = charge density

ω = angular frequency

CONTENTS

LIST OF FIGURES

LIST OF TABLES

Chapter I

INTRODUCTION

1.1 GENERAL

Although the dielectric properties of biological materials have been studied extensively and a considerable amount of data has been gathered, there is a continuing need to supplement the existing knowledge.

The need for research in this area is of increasing importance for various reasons. First, the information contained in dielectric properties helps to develop an understanding of the basic biophysical interaction mechanism of electromagnetic fields with living matter [1,2] which is, for instance, involved in the evaluation of the Specific Absorption Rate (SAR) of radio frequency or microwave frequency radiations for dosimetric calculations [3]. Such study is essential in evaluating potential health hazards from exposure to electromagnetic (EM) radiations [4] and to adequately determine safe levels for personnel exposed to such radiation. Secondly, this information is beneficial in biomedical applications such as developing effective therapeutic methods including electromagnetically (EM)-induced hyperthermia for cancer treatment, EM thawing of cryogenically preserved tissue and organs, and diathermy applica-

tions [5,6]. Finally, there are indications that diagnostic methods based on differences in the dielectric properties of normal and cancerous tissues are feasible [7].

Much activity has been spent on measuring human and animal tissues. The data available up to 1979 is tabulated in [8], while Stoy et al. [9] summarized the recent data of dielectric properties of mammalian tissues at low frequencies. Measurements of permittivities of various animal tissues are presented by several authors [10-13].

1.2 DIELECTRIC MEASUREMENTS : A REVIEW

Various methods for measuring the dielectric properties have been used. These methods can be divided into three major categories:

1. Cavity Perturbation Method
2. Loaded-line Method
3. Lumped-element Method

The cavity perturbation technique is based on measurement of the change in resonant frequency and Q factor of a cavity with and without a small dielectric sample [14,15]. Very little work has been done using this technique for biological materials because it requires tissue excision, making in-vivo dielectric measurements impossible. Moreover, the sample preparation is very difficult since its dimensions must be accurately known and small compared with the cavity.

In the loaded-line method, the sample is inserted into a waveguide or coaxial line and its complex permittivity is obtained from measuring the transmission and reflection scattering coefficients [15]-[17]. Like the cavity perturbation method, the sample must be excised, thus rendering in-vivo measurements impossible.

The lumped-element method is the technique which best lends itself to measurements of biological materials, thus receiving the attention of many researchers [18-28]. In this method, a lumped equivalent circuit is used to relate the admittance of a dielectric sensor to the permittivity of the sample. This approach has the advantage of providing closed-form expressions for the real and imaginary part of the permittivity as a function of the reflection coefficient, and measurements may be made using either resonant techniques or reflection techniques.

Tanabe and Joines [19] proposed a method based on the perturbation of the fringing field at the open end of a transmission line resonator by the unknown dielectric material. The open resonant system was represented by an L-C-G parallel lumped-element circuit and the permittivity was calculated from the measured changes in the resonant frequency and the Q factor.

In reflection techniques, the test sample permittivity is obtained from measurement of the reflection coefficient at the open end of the line or at a defined reference plane

(Fig. 1). The reflection coefficient may be measured by a slotted line or a network analyzer.

A variety of open and closed coaxial-line sensors and sample configurations have been developed for the lumped-element method. These range in configuration from placing a small sample inside the probe for measurement, to placing an open-ended line against a semi-infinite sample, depending on the measurement scheme as shown in Fig. 3.

There are some important points required for permittivity measurements as applied to biological materials:

1. Ability to perform living (in-vivo) tissue dielectric measurements;
2. Wide frequency range operation (typically 0.1 GHz to a few GHz);
3. Suitability for sample temperature control;
4. Ease of fabrication and sample preparation;
5. Convenient for both frequency domain and time domain measurements [18].

Among the various sample configurations shown in Fig. 3, only those in Fig. 3(a),(c),(i) and (k) have been studied extensively and only those in (i) and (k) have been used for in-vivo measurements. The ability to perform living (in-vivo) tissue dielectric measurements is important since factors such as temperature, blood flow, and possibly physiological changes between living and non-living tissues may influence the dielectric properties. Fig. 3(l) can also be

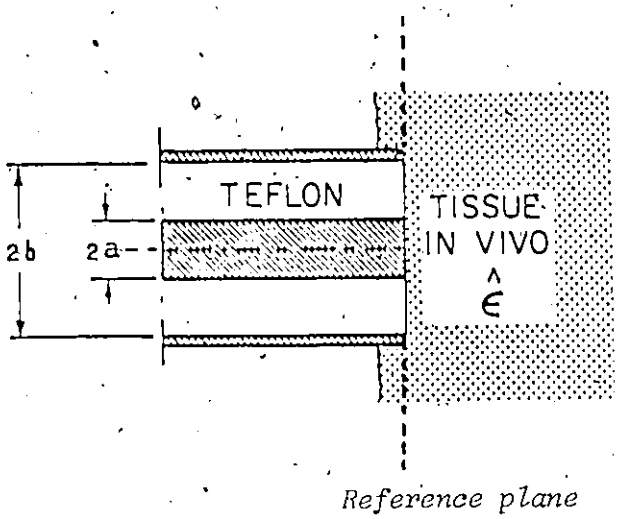

Figure 1: Geometry of open-ended coaxial line

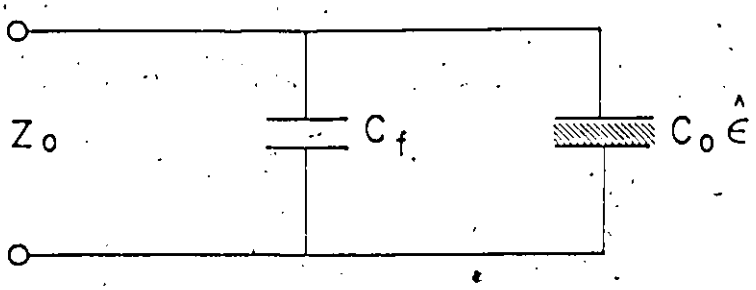

Figure 2: Equivalent circuit

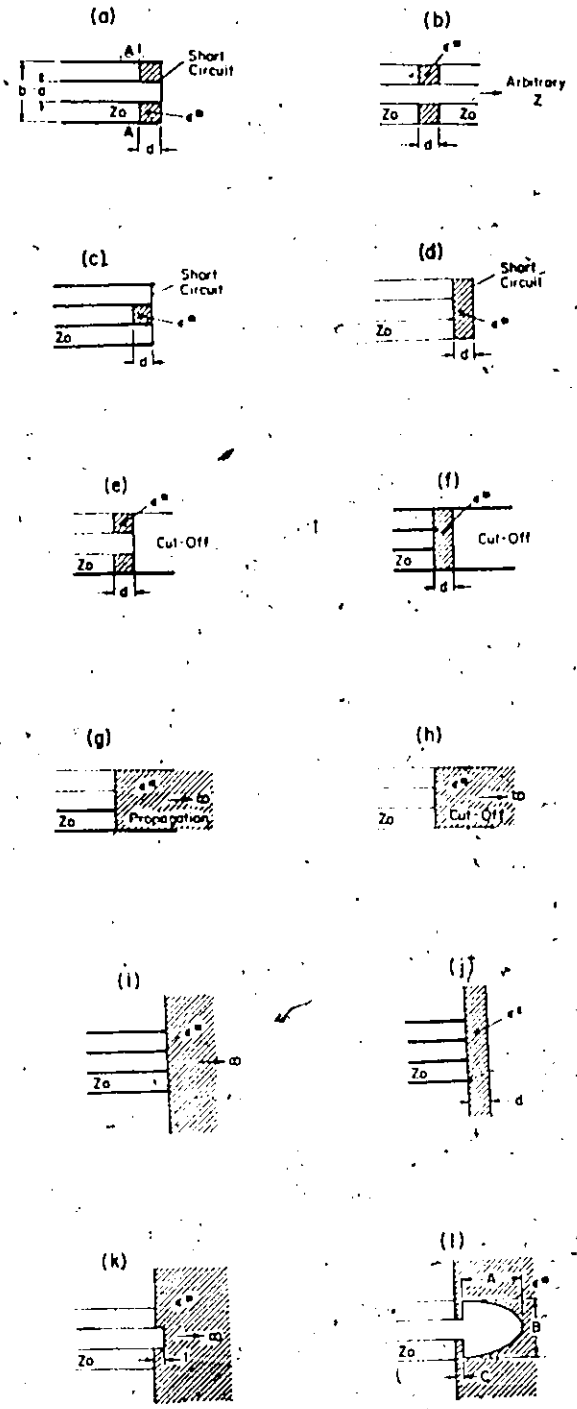

Figure 3: Sample configurations for measuring the permittivity.
(Permission from Ref. [18])

considered as suitable for in-vivo measurements. However it has several limitations, mainly because the input impedance, which is related to the permittivity of the sample, is very sensitive to the distance 'c' (see Fig. 3(l)). In addition, it does not offer any practical advantages comparing with the configurations in Figures 3(i) and (k) [18].

Burdette et al. [23] used a short monopole (Fig. 3(k)) with a limited-size ground plane to measure the dielectric properties in-vivo. The equivalent circuit of a short monopole immersed in a dielectric medium was used to relate the sample permittivity to the measured impedance of the sensor. The equivalent circuit is predominantly capacitive representing the storage of electric energy in the fringing fields while the small resistive component represents radiation losses. When the length of the monopole decreases, the configuration approaches that in Fig. 3(i) and the resistive component in the equivalent circuit becomes negligible. The sensor essentially becomes an open-ended coaxial line which provides several advantages over the short monopole, namely a less intrusive contact with the measured material, no necessity for accurately designed components, and a simpler equivalent circuit with which to relate the permittivity to the measured reflection coefficient.

The configuration in Fig. 3(i) was employed by Gajda [24] who included an additional shunt capacitance, independent of sample permittivity, in order to account for the fringing-

field inside the coaxial line. A numerical analysis of the capacitances of open ended coaxial sensors used for in-vivo permittivity studies of biological substances was performed in [27,28] and the related experimental measurements were presented in [10]-[13]. A more complete equivalent circuit including the effects of radiation from the open end of the sensor was proposed in [26].

Mosig et al. [25] presented a theoretical solution where the effects of radiation and higher order modes near the aperture of the open-ended coaxial line were taken into account. The permittivity was obtained from nomograms relating the reflection-coefficient to the relative permittivity of the sample in contact with the open end. The limitations of this method are that nomograms of relative dielectric constant and loss factor versus reflection-coefficient are required at each frequency and extensive numerical computations must be performed for each frequency and dielectric constant. In addition, these nomograms become increasingly complicated and time consuming to produce for materials with high permittivity, such as biological substances.

1.3 STATE OF THE PRESENT KNOWLEDGE

In recent years, measurement methods utilizing the sample holder shown in Fig. 3(i) have been used and analyzed extensively [23]-[28]. The relationship between the permittivity and the measured input reflection-coefficient of the open-ended coaxial line (Fig. 1) is derived on the basis of a simplified equivalent circuit represented in Fig. 2. This equivalent circuit is valid at frequencies where the dimensions of the line are small compared with the wavelength so that the open end of the line is not radiating and all the energy is concentrated in the fringe field of the line. The measurement reference plane is usually taken at the interface between the open end of the line and the test sample. The equivalent circuit consists of a section of uniform transmission line of characteristic impedance Z_o terminated by a capacitance $C(\hat{\varepsilon})$ and conductance $G(\hat{\varepsilon})$. It has been found that $G(\hat{\varepsilon})$ is negligible for most commonly used coaxial lines and over a large frequency range [26],[28]. Consequently it will be neglected in all further discussions.

Normally an infinite sample is used and a linear model relating the sample permittivity to the fringing capacitance is found to be a good approximation for large permittivities such as those encountered in biological materials [27],[28]. The fringing capacitance may be written as [18],[24]

$$C_T(\hat{\varepsilon}) = C_f + \hat{\varepsilon} C_o \qquad (1.1)$$

where $\hat{\varepsilon} = \varepsilon' - j\,\varepsilon''$ is the relative complex permittivity of the sample occupying the space outside the line. The constant term C_f represents the storage of energy in the fringing fields inside the teflon-filled part of the coaxial line while the linear term $\hat{\varepsilon}\,C_o$ represents the energy storage in the dielectric. The input admittance of the sensor can be written as:

$$Y = j\omega\,(C_f + \hat{\varepsilon}\,C_o) \tag{1.2}$$

$$= \frac{1}{z_0}\,\frac{1 - S_{11}e^{j\phi_{11}}}{1 + S_{11}e^{j\phi_{11}}} \tag{1.3}$$

where ω represents the angular frequency, S_{11} and ϕ_{11} represent the magnitude and phase of the reflection coefficient referenced to the plane of the open-circuit of the sensor.

From the above equations, closed-form expressions for the real and imaginary parts of the permittivity can be derived [18]

$$\varepsilon' = \frac{2\,S_{11}\sin(-\phi_{11})}{\omega\,C_0\,z_0\,[\,1 + 2\,S_{11}\cos(-\phi_{11}) + S_{11}^2]} - \frac{C_f}{C_o} \tag{1.4}$$

$$\varepsilon'' = \frac{1 - S_{11}^2}{\omega\;C_0\;z_0\;[\;1 + 2\,S_{11}\cos(-\phi_{11}) + S_{11}^2\;]} \tag{1.5}$$

where ε' denotes the relative dielectric constant and ε'' denotes the loss factor.

1.4 MOTIVATION AND PURPOSE OF STUDY

The objective of this thesis is to investigate the response of the open-ended coaxial sensor shown in Fig. 3(j) when utilized to measure the electrical properties of inhomogeneous dielectrics. It is shown in previous sections that only infinite samples (Fig. 3(i)) have been used, where the sample layer is thick enough to prevent reflection from the back end of the sample. However, in measurements of biological materials where parts of biological tissues have several finite or perhaps thin layers, for example skin, fat and muscle, it is important to take into consideration the effect caused by the material backing the thin-layer sample, and to estimate the minimum sample thickness required to simulate an infinite sample. The work presented in this thesis provides answers to these questions.

Investigation was begun by measuring thin layers of materials with known permittivities such as water, which has a high dielectric constant and low loss at low frequencies. In addition, its temperature can be easily controlled. Metallic and styrofoam sheets were used to limit the thickness of the water layer (see Fig. 4). The fringing capacitance was calculated numerically, using the Method of Moments, and measured experimentally, using an automated network analyz-

er. The result provides information about the upper and lower bounds of the sensor capacitance change in inhomogeneous media as compared with the homogeneous case. Thus, the depth of the interaction region of the sensor in dielectric measurements can be evaluated. In addition, the electric field intensity at the aperture of the sensor as well as in the dielectric material along the radial and axial lines give information about the minimum sample volume required for simulating an infinite sample. Also, the sensitive (high electric-field) regions of the sensor are identified from computations of the electric field in the region of the open end.

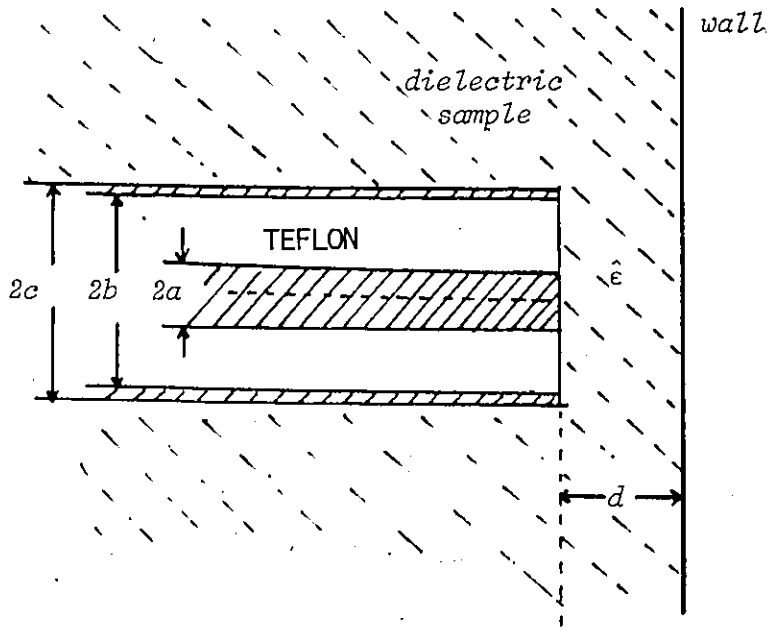

Figure 4: Geometry of an open-ended coaxial line sensor with a finite thickness sample.

Chapter II

NUMERICAL CALCULATION OF FRINGING CAPACITANCE

In this chapter a brief description of the Method of Moments and its use in calculating the static fringe-field capacitance of the coaxial-line sensor is presented. The geometry of the problem is assumed to consist of a coaxial sensor in contact with a layer of dielectric, backed by either a metal or air wall (shown in Fig. 4). The metal or air wall represents the two extremes of dielectric constant for the outer-most layer (i.e. infinity or unity), and gives rise to the upper and lower bounds in the capacitance. Two separate approaches were used to simulate the presence of the wall numerically. They are denoted here as the Finite Wall method and the Image Coeffiecient method and will be defined further on.

2.1 THE METHOD OF MOMENTS: THEORY

In order to solve a linear operator equation, the Method of Moments may be employed to transform such an equation into a system of linear algebraic equations which can be solved numerically. It is especially well adapted to the solution of static conductor-dielectric problems [29].

Consider the following inhomogeneous equation corresponding to a deterministic problem:

$$L(f) = g \tag{2.1}$$

where L is a linear operator, g is a known function and f is a function to be determined. Let the unknown function f be expanded in a linear combination of basis or expansion functions $f_1, f_2, \ldots, f_n, \ldots$ in the domain of L such that:

$$f = \sum_n \alpha_n f_n \tag{2.2}$$

where α are unknown constants and the domain of L is the set of all possible functions satisfying the boundary conditions accompanying the operator L. Substituting the expansion functions (2.2) into the operator equation (2.1) and using the linear property of the operator L gives:

$$\sum_n \alpha_n L(f_n) = g \tag{2.3}$$

$$n = 1,2,3,\ldots$$

An inner product is usually defined for the problem (2.1), where the integral of the product of two functions results in a scalar. Mathematically, it can be expressed as:

$$\langle f,g \rangle = \int_\Omega f^* \, g \, d\Omega' \tag{2.4}$$

which satisfies the following condition:

$$\langle f,g \rangle = \langle g,f \rangle^* \tag{2.5}$$

$$\langle \alpha_1 f + \alpha_2 g, u \rangle = \alpha_1 \langle f, u \rangle + \alpha_2 \langle g, u \rangle$$

$$\langle f^*, f \rangle = 0 \quad \text{for } f = 0$$

$$> 0 \quad \text{for } f \neq 0$$

where α_1 , α_2 are scalars and f,g,u are any functions. The symbol * denotes the complex conjugate. A set of weighting functions or testing functions w_m in the range of L is defined. The range of L is the space spanned by all functions g resulting from the operation. Taking the inner product of (2.3) with each w_m results in:

$$\sum_n \alpha_n \langle w_m, L f_n \rangle = \langle w_m, g \rangle \qquad (2.6)$$

$$m = 1,2,3...$$

The resulting algebraic system is solved for the unknown coefficients α_n. This set of equations can be written in matrix form as:

$$[L][\alpha] = [g] \qquad (2.7)$$

where

$$[L] = \begin{bmatrix} \langle w_1, L(f_1) \rangle & \langle w_1, L(f_2) \rangle & \cdots \\ \langle w_2, L(f_1) \rangle & \langle w_2, L(f_2) \rangle & \cdots \\ \cdots & \cdots & \cdots \\ \cdots & \cdots & \cdots \end{bmatrix}$$

$$\alpha = \begin{bmatrix} \alpha_1 \\ \alpha_2 \\ \vdots \\ \alpha_n \end{bmatrix} \qquad g = \begin{bmatrix} \langle w_1 , g \rangle \\ \langle w_2 , g \rangle \\ \vdots \\ \langle w_m , g \rangle \end{bmatrix}$$

If the matrix [L] is nonsingular, its inverse $[L]^{-1}$ exists and the α_n are then given by:

$$[\alpha] = [L]^{-1} [g] \tag{2.8}$$

The solution for f is obtained by using (2.2). It is important to select the appropriate sets of basis functions f_n and weighting functions w_m, used in (2.2) and (2.6), which will determine the solution to be exact or approximate. The w_m should be linearly independent and chosen so that the products $\langle w_m, g \rangle$ depend on relatively independent properties of g. Other factors which affect the choice of f_n and w_m are:

1. The accuracy of the solution desired;
2. The ease of evaluation of the matrix elements;
3. The size of the matrix that can be inverted;
4. The realization of a well-conditioned matrix [L].

Different schemes lead to various methods whose complete description can be found in [29].

The Method of Subsections involves the use of basis function f_n each of which exists only over a single subsection

of the domain of f. Then each α_n of the expansion (2.2) effects the approximation of f only over a subsection of the region of interest. This procedure often simplifies the evaluation and the form of the matrix [L]. In the collocation (point matching) method, Dirac delta functions are used as weighting functions. When the basis functions are chosen to be the same of the weighting functions, this procedure is known as Galerkin's method. The Method of Subsection in conjunction with collocation (point-matching) lends itself to solve the conductor-dielectric coupled integral equations effectively [28].

2.2 APPLICATION TO THE PROBLEM

2.2.1 Finite Wall method

The open-ended coaxial line sensor terminated with finite thickness sample to be analyzed in this section is shown in Fig. 4. . Two essential parameters to be determined are the fringe-field capacitance of the sensor and the electric field distribution with varying sample thickness 'd'. The Method of Moments is employed to solve for the unknown charge distribution on the conductors and the dielectric interfaces which then may be used to calculate all the other quantities. The metal wall backing the sample may be considered as an additional conductor and the air wall is treated as another dielectric interface. The coupled integral equations relating the free surface charge distribution

on conductors and the bound surface charge distribution on dielectric interfaces, due to a potential distribution $\Phi(s)$, are given by [31,32]

$$\int_{S_c+S_I} \sigma(s')\, G(s|s')\, ds' = \Phi(s) \qquad (2.9)$$

$$s \text{ on } S_c$$

$$\frac{\varepsilon_L + \varepsilon_{L+1}}{2}\sigma(s) + (\varepsilon_L - \varepsilon_{L+1}) \int_{S_c+S_I} \sigma(s')\, \frac{\partial G}{\partial n}(s|s')\, ds' = 0 \qquad (2.10)$$

$$s \text{ on interface between } \varepsilon_L,\ \varepsilon_{L+1}$$

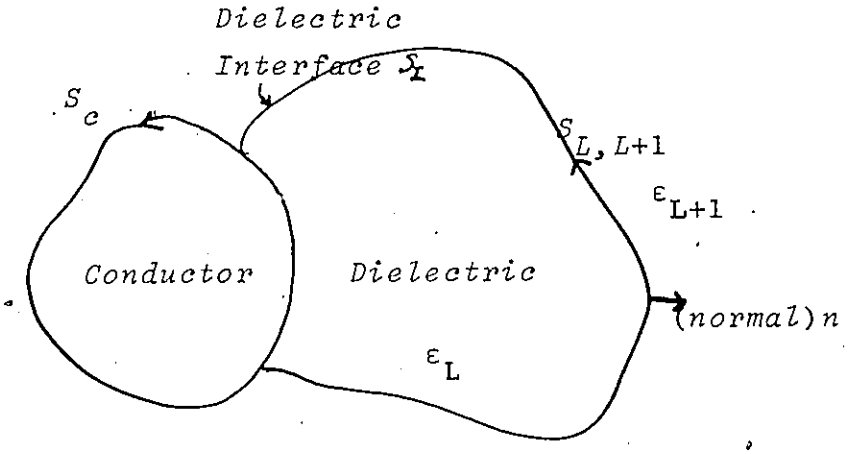

Figure 5: Orientation of normal vectors on the interface between different dielectric media.

where $G(s|s')$ is the scalar potential Green's function, S_c and S_I denote conductor surface and dielectric interfaces, respectively, $\sigma(s)$ is the charge density, and ε_L and ε_{L+1} are the two permittivities of the dielectric regions where the normal n is directed from region L to region L+1 (Fig.

5). In the rotationally symmetric system, the Green's function and its normal derivative are expressed in terms of the complete elliptic integral of the first kind and its derivative [31].

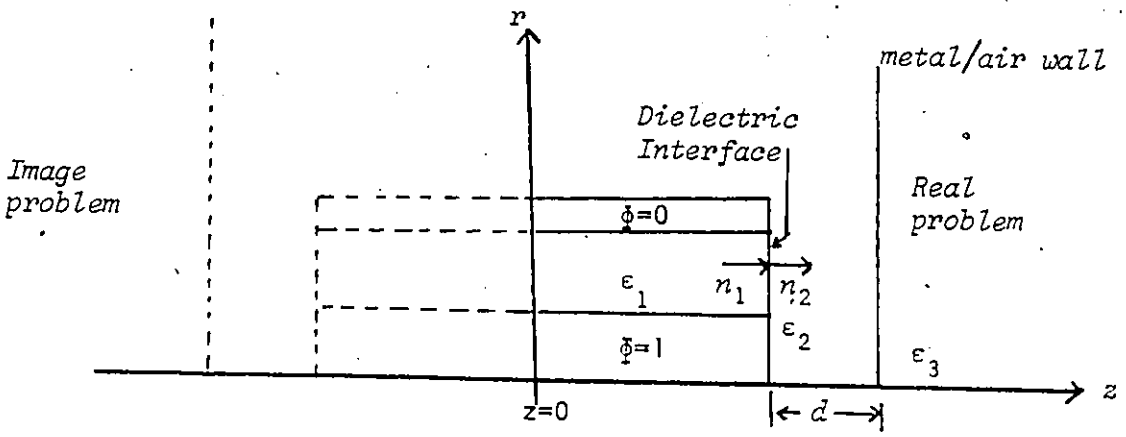

Figure 6: Configuration of the real and image problems for MOM solution of an open-ended line sensor.

The potential on the inner conductor is held at one volt and zero volts on the outer conductor and the metal wall. The Method of Moments is applied to equations (2.9) and (2.10) by dividing all surfaces into subsections and assuming a uniform charge density of unknown amplitude on each subsections. The discretized integral equations are then enforced at the midpoint of each subsection, yielding a system of algebraic equations for the unknown charge-pulse am-

plitudes. This approach is known as the Method of Subsections with point matching or collocation. It is equivalent to using pulse expansion and Dirac or impulse weighting functions.

In order to approximate an infinite coaxial line in the negative z-direction (see Fig. 6), the Method of Images is employed [28]. The line must be selected long enough in order that the charge distribution far from the aperture is approximately uniform, as is expected for an infinite uniform coaxial line. The charge distribution on the real conductors and interfaces and their mirror images about $z = 0$ are found. However, due to symmetry, the image elements do not increase the number of unknowns.

The 'Finite Wall Method' is not a standard name for this particular method since it is a method involving the application of the Moment Method to account for the presence of the wall. The metal/air wall may be solved likewise as for the conductors and dielectric interface of the coaxial line by using the same expressions given in (2.9) and (2.10). However, it is convenient to give this approach a name so that one may be able to distinguish and describe the two different approaches used specifically to deal with the wall, namely the Finite Wall Method and the Image Coefficient Method. For simplicity, the barrier separating the two different dielectric samples is called a 'wall', for example, the metal wall or air wall.

The first method is called the Finite Wall Method because only a finite space of the wall is used in the numerical computation. The extent of the wall must be chosen properly in order to include almost all of the energy stored in it. This can be done by increasing the dimension of the wall progressively during computation until the computed capacitance converged to a single value. In this approach, the finite wall is treated simply as an additional conductor or dielectric interface of finite dimensions. The wall is subsectioned as with all other boundaries and causes an increase in the number of unknowns to be solved. On the other hand, no computation of the wall is necessary for the Image Coefficient Method because the series of the image charges is equivalent to the existence of the infinite wall.

The capacitance is evaluated by integrating the charge over one of the conductor surfaces and dividing by the potential difference V ,

$$C_{T1} = \frac{1}{V} \int_{s_c} \varepsilon(s) \frac{\partial \Phi(s)}{\partial n} ds \qquad (2.11)$$

where $\frac{\partial \Phi}{\partial n}$ is the potential gradient terminating on the conductor and $\varepsilon(s)$ is the permittivity of the dielectric contacting the surface. The product of the two is the normal electric flux density or charge density $\sigma(s)$. The net fringe-field capacitance is determined by subtracting the contribution due to the TEM fields inside the line, given by:

$$C_{TEM} = \frac{2\pi \epsilon_1 L}{\ln\left(\frac{b}{a}\right)} \qquad (2.12)$$

where L is the length of the coaxial line, ϵ_1 is the permittivity of the dielectric inside the line, a and b are the inner and outer-conductor radii, respectively. A complete numerical procedure and detailed description regarding the computation of sensor capacitance with infinite sample can be found in [28].

2.3 APPLICATION OF IMAGE COEFFICIENT METHOD TO INHOMOGENEOUS DIELECTRIC PROBLEM

In cases where dielectric boundaries form infinite planes, the method of Images may be exploited to reduce the overall number of unknowns. Using the Image Coefficient Method [30], the infinite dielectric wall may be represented mathematically as a convergent series in the Green's function of integral equation, thereby eliminating the need to subsection the wall.

2.3.1 Image Coefficient

Let the halfspace $x < 0$ be filled with a homogeneous dielectric of permittivity ϵ_1, and let a line charge of q coulombs per meter lie at $(x_0, 0, z)$, as shown in Fig. 7. This charge will produce an electric flux uniformly in all radial directions. At the dielectric surface, some fraction $k\psi_1$ of the flux will fail to penetrate into the dielectric, while the remainder $(1 - k)\psi_1$ must continue in the dielec-

tric material. The reflected flux $k\psi_1$ returns from the dielectric surface with an angle α_2. In order to fulfill the boundary conditions, the normal component of flux density requires that:

$$(1-K)\psi_1 \sin\alpha_1 = \psi_1 \sin\alpha_1 - K\psi_1 \sin\alpha_2 \qquad (2.13)$$

where the angles of incident and reflected flux line must be equal. In addition, the continuity of the tangential electric component is possible only if:

$$\frac{1}{\varepsilon_1}(1-K)\psi_1 \cos\alpha_1 = \frac{1}{\varepsilon_0}\psi_1 \cos\alpha_1 + \frac{1}{\varepsilon_0} K\psi_1 \cos\alpha_2 \qquad (2.14)$$

Therefore an image coefficient K may be expressed as:

$$K = \frac{\varepsilon_0 - \varepsilon_1}{\varepsilon_0 + \varepsilon_1} \qquad (2.15)$$

The equality of angles of incidence and reflection leads to an apparent existence of images [30]. Using the image coefficient K, the potential due to the series of the image charges can be obtained as shown in the next section.

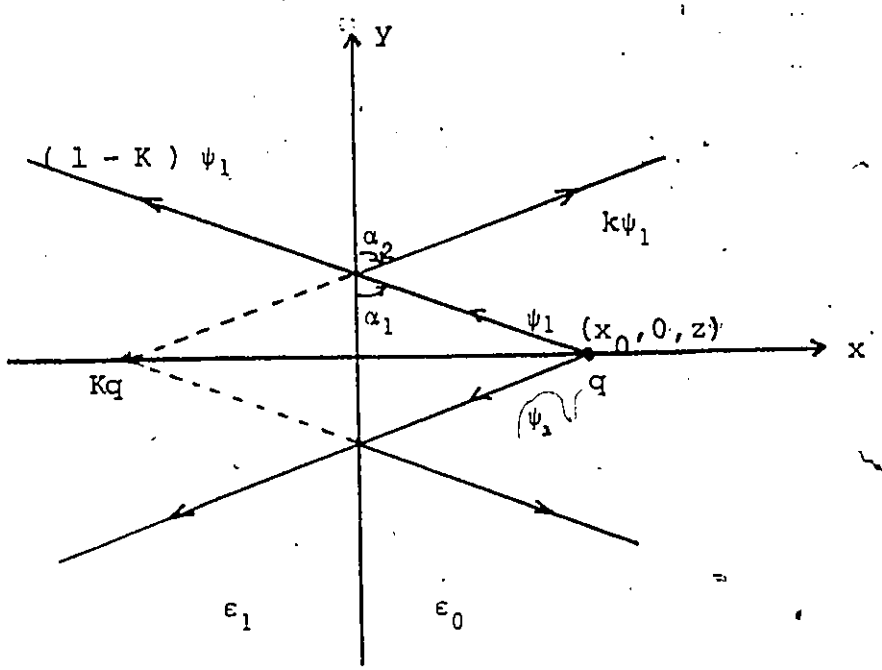

Figure 7: A line charge and its flux lines.

2.3.2 Dielectric Wall

The image-coefficient method described in the previous section is now applied to a point charge located in a region bounded by infinite dielectric sheets. In this case, every reflected flux line is subject to further partial reflection at either plane 1 or plane 2, - and this will continue on to infinity. This process is illustrated in Fig. 8 by a simple graphical construction.

The resulting flux-line representation of Fig. 8 is valid throughout the r-z plane and the image representations permit analytic expressions for the potential to be written with great ease. It can be shown that the sum of the strengths of all image charges forms a series which natural-

ly converges to zero. The potential due to a point charge located at $(r,z) = (r_0,z_0)$ inside the region between two bounded walls as shown in Fig. 8 may be expressed as [30]:

$$\Phi(r,z) = \frac{1}{4\pi\varepsilon_3}\left[\frac{q}{\sqrt{(r+r_0)^2 + (z-z_0)^2}}\right.$$

$$+ q\sum_{n=1}^{\infty}\frac{K^n}{\sqrt{(r+r_0)^2 + [z-2nd+(-1)^{n+1}z_0]^2}}$$

$$\left. + q\sum_{n=1}^{\infty}\frac{K^n}{\sqrt{(r+r_0)^2 + [z+2nd+(-1)^{n+1}z_0]^2}}\right] \quad (2.16)$$

where the image coefficient is:

$$K = \frac{\varepsilon_2 - \varepsilon_3}{\varepsilon_2 + \varepsilon_3} \quad (2.17)$$

In the limiting case where the dielectric constant ε_3 becomes very large and approaches infinity, none of the flux arriving at the dielectric interface is able to penetrate. Therefore, this totally reflective boundary gives a negative image coefficient $K = -1$, which is equivalent to replacing the dielectric wall with a metallic plate. A different approach and explanation will be given in the following section to show that the equation derived in (2.16) is valid also for metal wall.

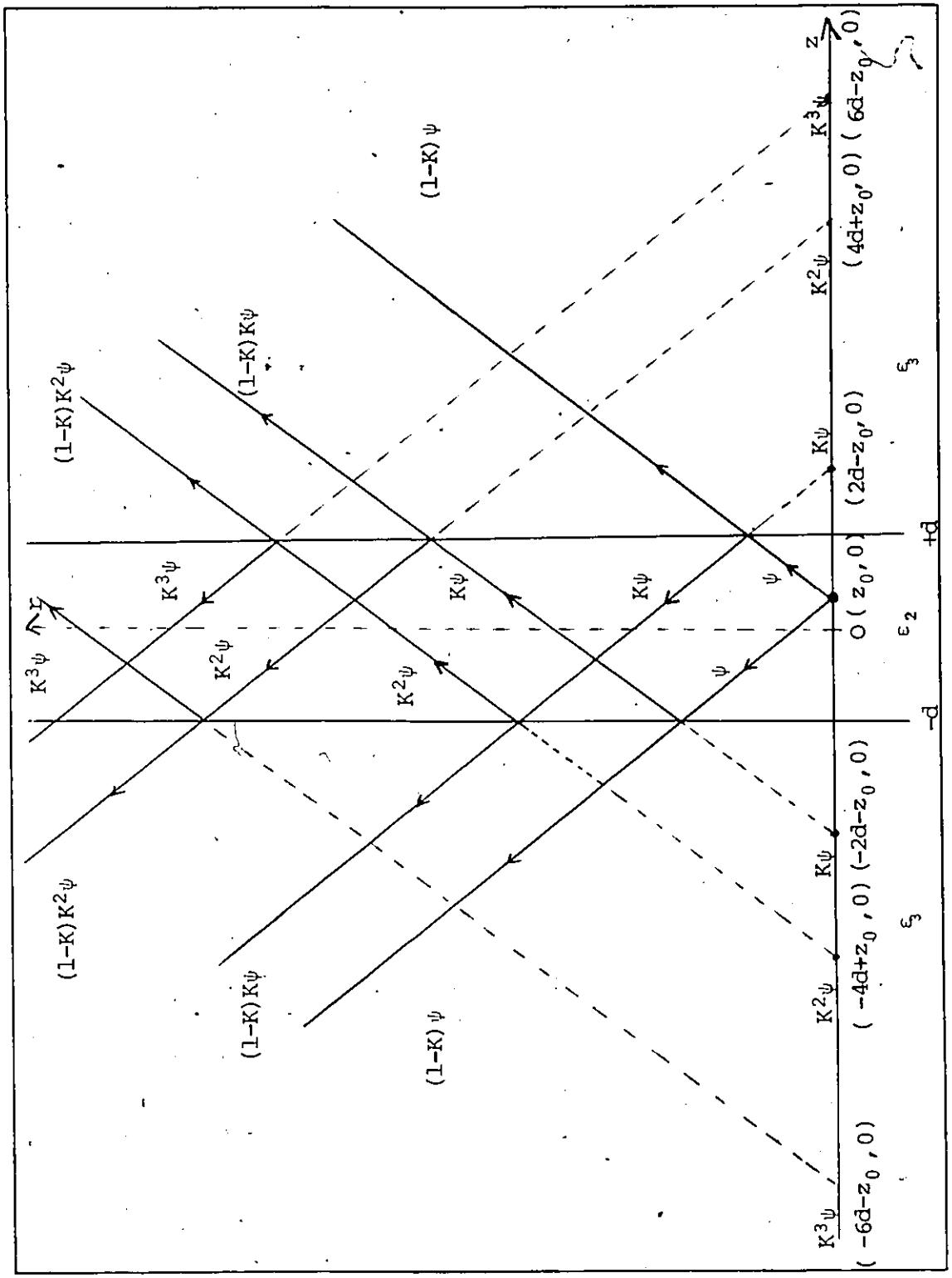

Figure 8: Flux lines due to a charge in an infinite dielectric sandwich.

2.3.3 Metal Wall

In the case where a charge is located between two metallic planes, a different approach to finding the equivalent image charges and the resulting potential function may be used. Let's assume that the plane is grounded and hence is held at zero potential. Consider the following system consisting of a point charge q lying between two infinite ground planes as shown in Fig. 9.

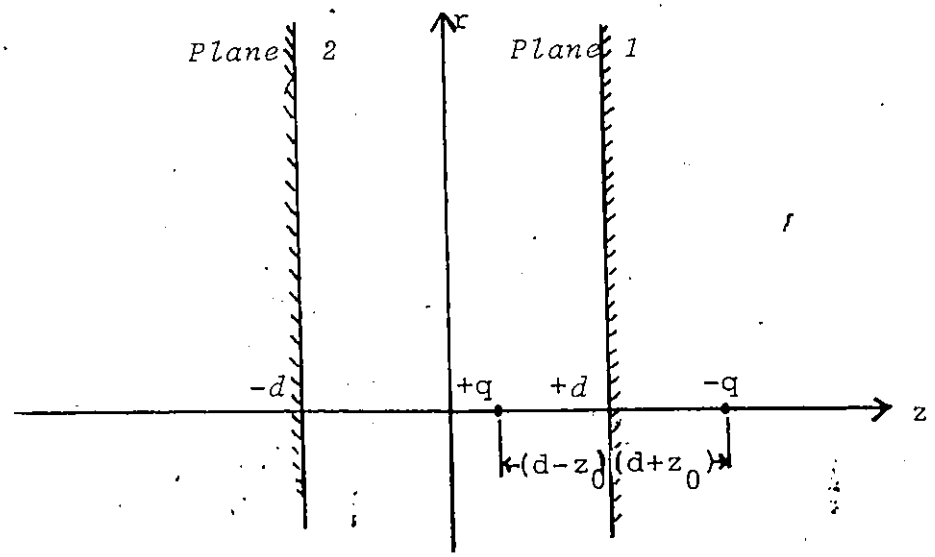

Figure 9: A point charge q with its image charge.

The effects of the ground planes may be described by the potential due to an infinite series of image charges. The location of these image charges may be determined by alternately enforcing the potential on both ground planes to be equal to zero. For instance, on plane 1, the potential can

be made zero by placing a negative image charge opposite the real one as shown. Calculating the potential on plane two then gives:

$$\Phi_2(r,z) = \frac{1}{4\pi\epsilon_2}\left[\frac{q}{\sqrt{r^2 + (d + z_0)^2}} - \frac{q}{\sqrt{r^2 + (3d - z_0)^2}}\right] \quad (2.18)$$

The fact that the above expression is not identically equal to zero implies that two image charges must be added which are located a distance $(d + z_0)$ and $(3d - z_0)$ to the left of plane 2, to ensure the potential on plane 2 to be zero.

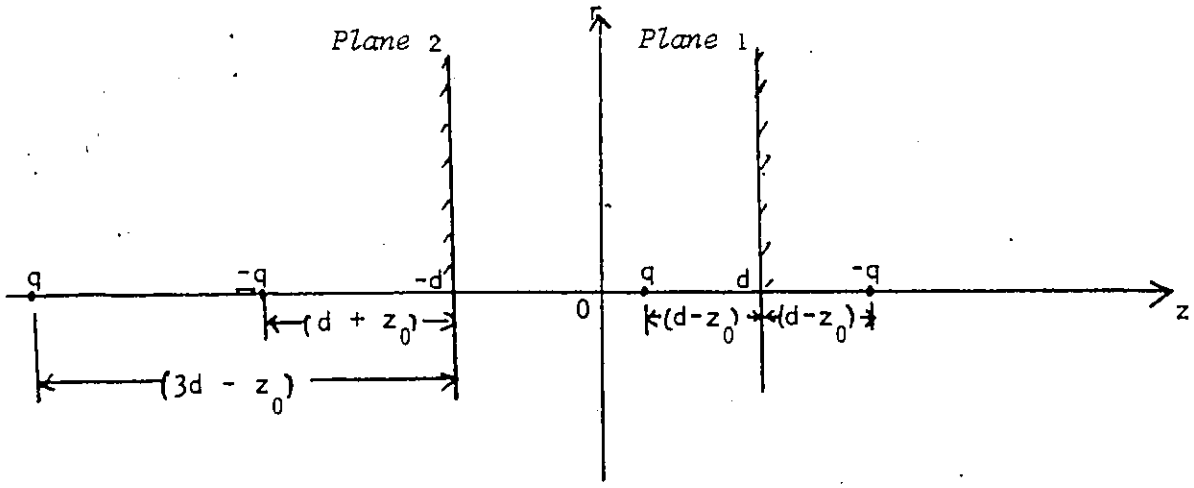

Figure 10: Two additional image charges located at the left plane.

Calculating the potential on plane 1 again, gives:

$$\Phi_1(r,z) = \frac{1}{4\pi\epsilon_2}\left[\frac{q}{\sqrt{r^2 + (d-z_0)^2}} - \frac{q}{\sqrt{r^2 + (d-z_0)^2}} - \right.$$

$$\left. - \frac{q}{\sqrt{r^2 + (3d + z_0)^2}} + \frac{q}{\sqrt{r^2 + (5d - z_0)^2}}\right] \quad (2.19)$$

The above equation indicates that two more image charges must be placed a distance $(3d + z_0)$ and $(5d - z_0)$ to the right of plane 1, in order to obtain zero potential.

This procedure continues on to infinity producing the following series of image charges (see Fig. 11). The potential due to this infinite series of charges is then expressed as:

$$\phi(r,z) = \frac{1}{4\pi\epsilon_2}\left[\frac{q}{\sqrt{r^2 + (z - z_0)^2}} + \sum_{n=1}^{\infty}\frac{q(-1)^n}{\sqrt{r^2 + [z - 2nd + (-1)^{n+1} z_0]^2}} + \sum_{n=1}^{\infty}\frac{q(-1)^n}{\sqrt{r^2 + [z + 2nd + (-1)^{n+1} z_0]^2}}\right] \qquad (2.20)$$

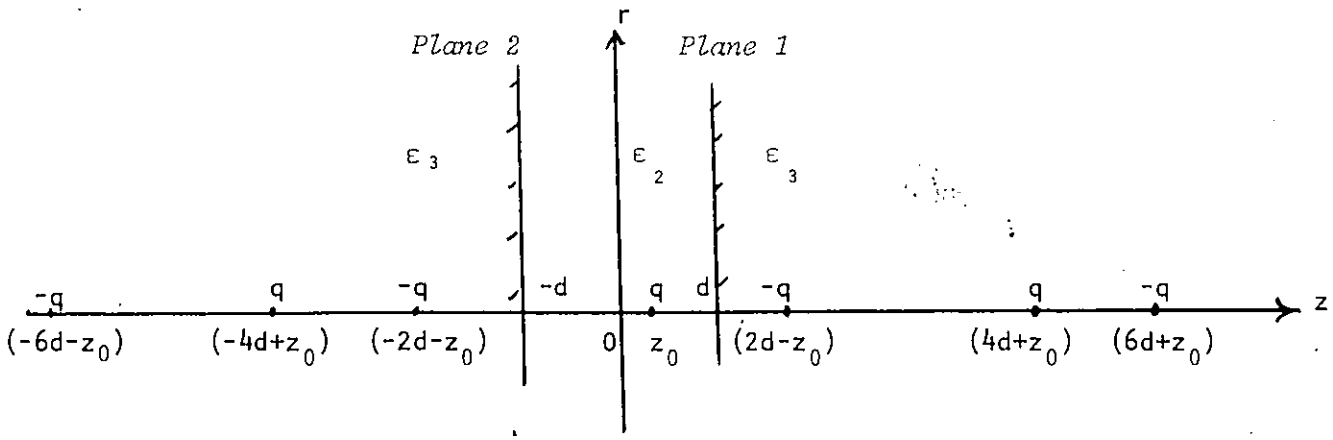

Figure 11: A real charge with its infinite series of image charges.

The equation (2.20) derived is then identical to that expressed in (2.16) with K = -1 and $r_0 = 0$. If the finite thickness dielectric sample is bounded by air or free space, the image coefficient K is given as:

$$K = \frac{\varepsilon_2 - \varepsilon_3}{\varepsilon_2 + \varepsilon_3} \qquad (2.21)$$

where the normalized free space permittivity ε_3 is equal to unity.

Since the series of image charges is equivalent to having two ground planes, the above expression represents the potential due to a point charge located at $(r,z) = (0,z_0)$, between two ground planes. If the charge does not lie on the axis but rather at a point (x_0, y_0, z_0) then r^2 is replaced by $(x - x_0)^2 + (y - y_0)^2$, in the above derivation.

2.3.4 Green's Functions

For application to rotationally-symmetric systems, the potential due to a point charge must be replaced by the potential due to a uniform ring of charge. The Green's function therefore represents the potential at a point (r,z) due to a ring of charge of radius r' and centre located at z' as in Fig. 12.

The distance between the observation point P and the source point P' is given by:

$$R = \sqrt{(x-x')^2 + (y-y')^2 + (z-z')^2}$$

$$= \sqrt{(r-r')^2 + (z-z')^2 - 4\, r\, r' \cos^2 \frac{\theta}{2}} \qquad (2.22)$$

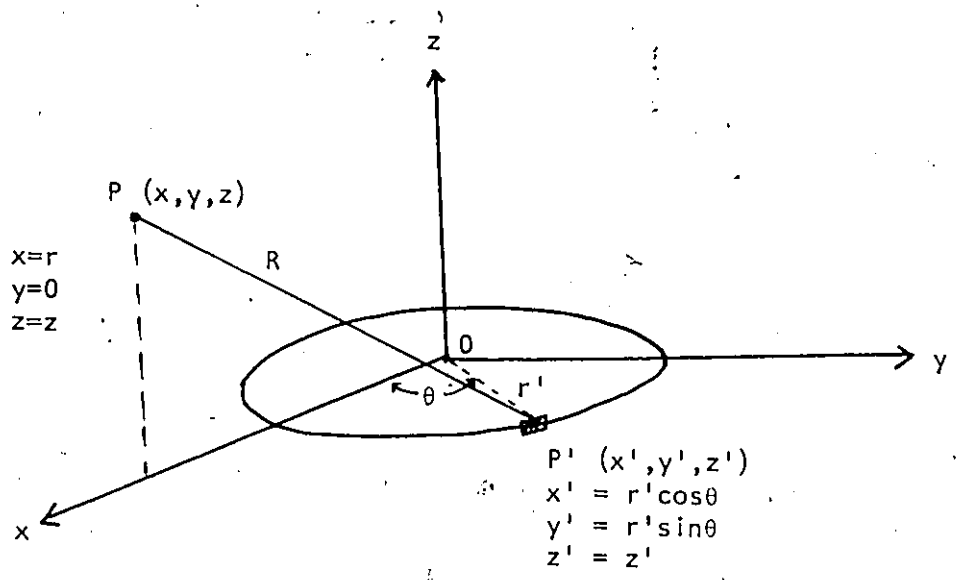

Figure 12: Infinitesimal ring used in derivation of the Green's function.

The rotationally-symmetric Green's function for a single ring of charge is written as [31]:

$$G(r,z) = \frac{1}{4\pi\varepsilon} \int_0^{2\pi} \frac{1}{\sqrt{(r + r')^2 + (z - z')^2 - 4rr' \cos^2 \frac{\theta}{2}}} \, d\theta$$

$$= \frac{1}{\pi\varepsilon} \frac{1}{\sqrt{(r + r')^2 + (z - z')^2}} E(k) \qquad (2.23)$$

where

$$k^2 = \frac{4 r r'}{(r + r')^2 + (z - z')^2}$$

and E(k) is the complete elliptic integral of the first kind. defined as:

$$E(k) = \int_0^{\frac{\pi}{2}} \frac{d\theta}{\sqrt{1 - k^2 \sin^2 \theta}} \qquad (2.24)$$

When a wall is placed in close proximity to the open end of the sensor, the Green's function for cylindrical systems can now be found by considering a real ring of charge with radius r' located at z = z' and the infinite series of image charge rings due to the two infinite walls as shown in Fig. 13.

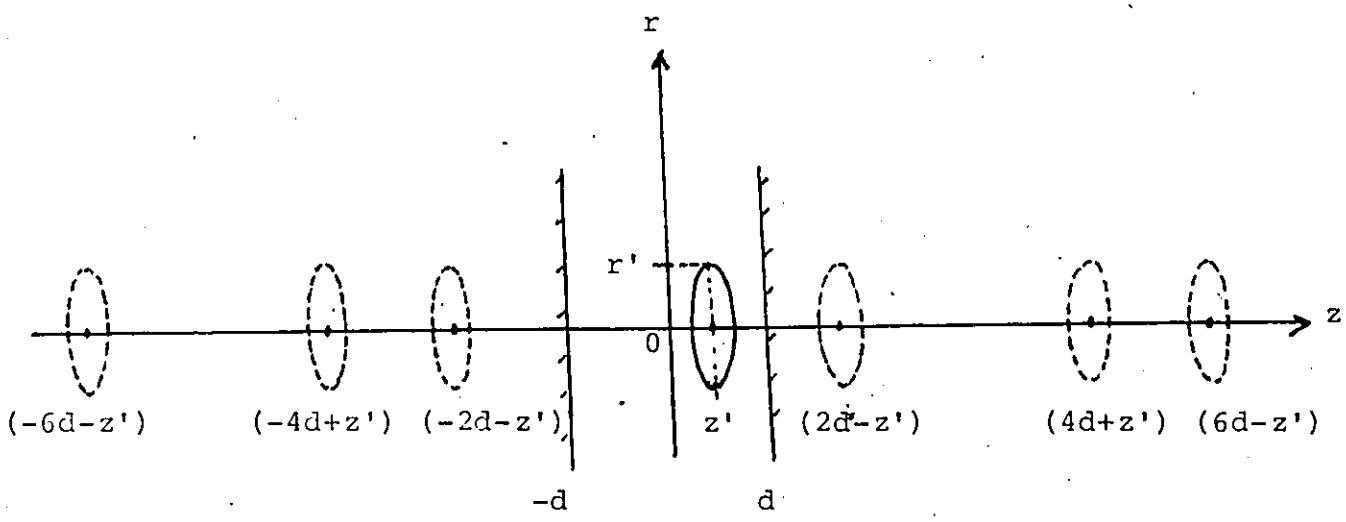

Figure 13: Real ring of charge and its mirror images.

The Green's function is thus expressed as:

$$G(r,z \mid r',z') = \frac{1}{\pi\varepsilon}\left[\frac{1}{\sqrt{(r + r')^2 + (z - z')^2}} E(k) \right.$$

$$+ \sum_{n=1}^{\infty} \frac{K^n}{\sqrt{(r + r')^2 + [z - 2nd + (-1)^{n+1} z']^2}} E(\alpha_n)$$

$$\left. + \sum_{n=1}^{\infty} \frac{K^n}{\sqrt{(r + r')^2 + [z + 2nd + (-1)^{n+1} z']^2}} E(\beta_n) \right] \qquad (2.25)$$

where

$$k^2 = \frac{4\, r\, r'}{(r + r')^2 + (z - z')^2}$$

$$\alpha_n^2 = \frac{4\, r\, r'}{(r + r')^2 + [z - 2nd + (-1)^{n+1} z']^2}$$

$$\beta_n^2 = \frac{4\, r\, r'}{(r + r')^2 + [z + 2nd + (-1)^{n+1} z']^2}$$

where $E(k)$, $E(\alpha_n)$, $E(\beta_n)$ are the complete elliptical integrals of the first kind.

2.3.5 Organization of Solution

To implement a solution by the method of subsections, the real conductors and finite interface in Fig. 14 are divided into subsections, numbered from i = 1 to i = n for conductors and i = n+1 to i = n+m for the interface.

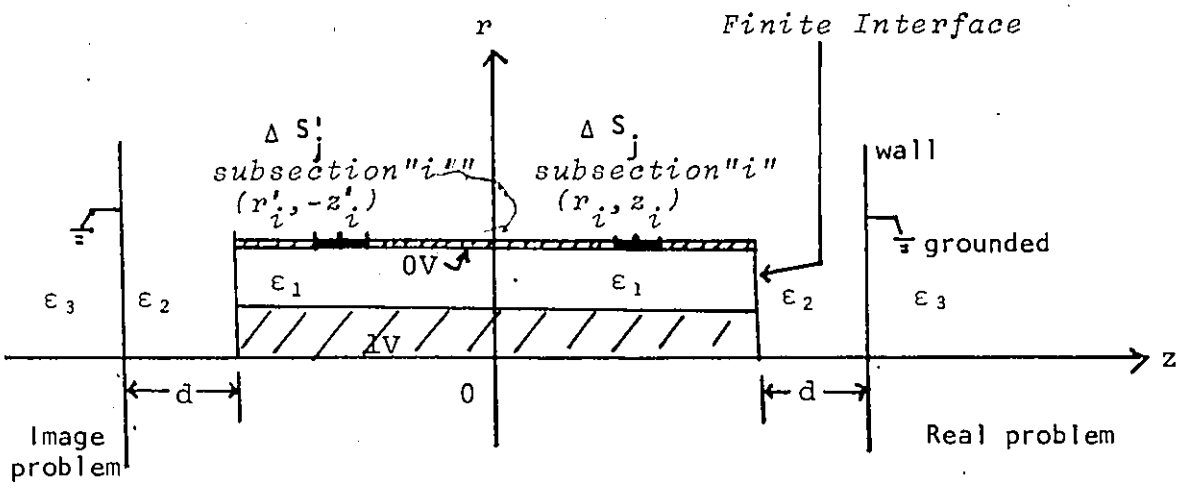

Figure 14: The coaxial sensor with wall presence and its mirror image.

Since it is symmetric about z = 0, i.e. $\Delta S_j' = \Delta S_j$, only one half of the problem is required to be subsectioned. The infinite metal or air wall is not subsectioned since it is taken into account in the Green's function. Using point matching techniques, the coupled integral equations in (2.9) and (2.10) become:

$$\sum_{j=1}^{n+m} \sigma_j \left[\int_{\Delta s_j} G(s_i|s')\, ds' + \int_{\Delta s_j'} G(s_i|s')\, ds' \right] = \Phi(s_i) \qquad (2.26)$$

$$i = 1,2,\ldots\ldots,n.$$

$$j = 1,2,\ldots\ldots,n+m.$$

$$\frac{(\varepsilon_L + \varepsilon_{L+1})}{2}\sigma_i + (\varepsilon_L - \varepsilon_{L+1})\sum_{j=1}^{n+m}\sigma_j\left[\int_{\Delta s_j}\frac{\partial G}{\partial n}(s_i|s')\,ds' + \int_{\Delta s'_j}\frac{\partial G}{\partial n}(s_i|s')\,ds'\right] = 0$$

$$i = n+1, n+2, \ldots\ldots, n+m.$$

$$j = 1, 2, \ldots\ldots\ldots, n+m. \quad (2.27)$$

The fringe-field capacitance can be calculated once the charge density is known. Equation (2.11) is then evaluated as follow:

$$C_{TI} = \frac{1}{V}\sum_{i=1}^{k}\sigma_i\,\varepsilon_i\int_{\Delta s_i} ds \quad (2.28)$$

The net fringe-field capacitance which is equivalent to the C_T in (1.1) may be calculated:

$$C_T = C_{TI} - C_{TEM}$$

where C_T is the total capacitance, σ_i is the pulse amplitude in units of C/m^2 and the summation is over all positively or negatively charged subsections lying on conductors.

In a rotationally-symmetric system, the total stored electric energy W_E is given by

$$W_E = \frac{1}{2}\int_{\Omega}\varepsilon|\nabla\phi|^2\;2\pi\,r\,dr\,dz \quad (2.29)$$

and it can also be expressed in terms of the capacitance as:

$$W_E = \frac{1}{2}C\,V^2 \quad (2.30)$$

where V is the potential difference between the two conductors.

The electric field along the radial and axial directions may be calculated as follow:

$$\vec{E} = -\vec{\nabla}\,\Phi \tag{2.31}$$

$$E_r = -\frac{\Delta\phi}{\Delta r} \tag{2.32}$$

$$E_z = -\frac{\Delta\phi}{\Delta z} \tag{2.33}$$

$$E_{Total} = \left|\sqrt{E_r^2 + E_z^2}\right| \tag{2.34}$$

where E_r and E_z are the electric field in the r and z direction, respectively, and E_{Total} is the resultant field of the two components. Thus the electric field along the axial and radial lines can be mapped which will be shown in the next chapter.

Chapter III

NUMERICAL RESULTS

In this chapter, the numerical results obtained from the Finite Wall Method and the Image Method are compared and analysed. Variations of the fringe-field capacitance as a function of displacement of the wall gives information about the effects of finite thickness samples backed by a wall or bi-layered samples. In addition, the minimum sample volume required to simulate an infinite sample can be estimated. Finally, the electric field intensity at the aperture of the coaxial line as well as in close proximity to the line is mapped, showing the sensitive (strong electric-field) regions of the sensor in contact with the sample, which may be useful for measurement purposes.

3.1 PROGRAM DESCRIPTION

A FORTRAN program of the Moment Method used for calculating the fringe-field capacitance of the infinite samples [28] was modified for use in an inhomogeneous dielectric problem. This program solved the coupled integral equations (2.9) and (2.10) using a subsectional basis and point-matching method in a rotationally-symmetric system. The IMSL subroutine packages [33] were employed for the calculation

of the elliptic integral function and solution of the final system of equations. The matrix inversion routine is capable of handling large-sized matrices with full storage mode and produces high accuracy solutions. Also, it requires less CPU time as compared with the Gauss elimination approach.

The derivative of the Green's function was obtained using the finite differences instead of the backward difference approximations originally proposed in [28]. Two separate subroutines were used to replace the subroutine of the Green's function and its derivative given in [28]. The first routine computes the Green's function containing the complete elliptic integral, while the other calculated its derivative. This approach eliminates the complication of numerical and analytical derivation of the Green's function and provides flexibility for any modification to the Green's function without reprogramming the subroutine. For the program utilizing the Image Coefficient Method, the Green's function subroutine was modified to accept the infinite series in (2.25). Notice that subsections for the wall are not needed for this case since the converging series of image charges represents the infinite wall. All operation were performed with double precision (8 word) arithmetic on an Amdahl 470/V7A computer and the listings are presented in appendix A.

3.2 COMPARISON BETWEEN FINITE WALL METHOD AND IMAGE COEFFICIENT METHOD

The sensor configuration utilized for analysis is shown in Fig. 14 and a comparison of the total capacitance obtained from the two different approaches is tabulated in Tables 1 and 2. Table 1 gives values of the total capacitance normalized to the free-space permittivity and aperture dimension (b-a) for various sample permittivities. These values of $C/\varepsilon_0(b-a)$ apply to any size of 50-Ω air-filled coaxial line for which the ratio b/a is equal to 2.303, where b and a are the outer and inner conductor radii, respectively. The relative permittivity used for filling the space between the coaxial line and the wall ranges from 10.0 to 60.0, where the wall is located at a distance of twice the inner conductor radius.

Table 2 shows a comparison of the results of the two methods for distances between the tip of the sensor and the wall (denoted by 'd') ranging in value from a to 30a, where a is the inner conductor radius (see Fig. 14). The dimensions of the semi-rigid line are taken from standard manufacturers data where c/a = 3.925 and b/a = 3.268 for teflon-filled line ($\varepsilon_r = 2.05$).

For the finite wall analysis, the necessary dimension of the wall required for the capacitance to converge had a radius of approximately seven times the inner-conductor radius. The dimension was determined by successively increasing the region of the wall during computation until the change

TABLE 1

Comparison of C_T/ε_0 (b-a) versus ε_r for a 6.4-mm air-line obtained from Image Coefficient and Finite Wall Method.

d/a = 2

ε_r	C_T/ε_0 (b-a)			
	Metal wall		Air wall	
	Image Coef. Method	Finite Wall Method	Image Coef. Method	Finite Wall Method
10	40.428	40.567	35.605	35.616
20	79.742	80.190	70.027	70.223
40	158.271	159.339	138.793	139.360
60	236.776	238.463	207.540	208.539

in the capacitance between consecutive runs became less than 0.1%. A sufficient length of coaxial line to ensure that the charge distribution on both inner and outer conductors to be approximately uniform in the vicinity of z = 0 is found to be equal to eight times the inner conductor radius [28]. The minimum number of subsections required for the wall was seven where it was found that doubling the number of subsections produce only 0.1% difference in the total capacitance value. It was also observed that further increasing the size and the number of subsections of the wall used above produced negligible change in the capacitance. For

TABLE 2

Comparison of the two methods of normalized fringing capacitance versus position of the wall for a 6.4-mm line.

water $\varepsilon_r = 80$

d/a	$C_T / \varepsilon_0(b-a)$			
	Metal Wall		Air Wall	
	Image Coef. Method	Finite Wall Method	Image Coef. Method	Finite Wall Method
1	220.74	223.92	113.39	113.78
2	176.33	177.82	143.45	143.88
4	161.65	162.52	153.81	154.54
6	158.80	159.85	155.62	156.45
8	158.32	158.92	155.85	157.12
12	157.65	158.29	156.47	157.57
30	157.37	157.88	156.63	157.79

example, tripling the size and number of subsections of the wall only gives less than 0.1% difference in the result. The conductor and interface of the coaxial line required at least 58 and 17 subsections, respectively [28].

For the image coefficient analysis, the infinite series in (2.25) converges rapidly. Only two terms in each series are necessary to ensure convergence within 1%. Each term requires an additional fifty seconds of computer time for a solution.

3.2.1 Discussion

In terms of the CPU time, the Finite Wall Method requires 40 seconds to run for a typical problem compared with 103 seconds for the Image Coefficient Method. More time is needed for the Image Coefficient Method because its Green's function contains several series to simulate the image charges. Although the Finite Wall Method necessitates more unknowns and thus storage requirements, these factors are trivial in both the programming and executing process. The IMSL routines, capable of handling large size matrices with good accuracy, requires only a few seconds of execution time. Therefore, it is recommended to use the Finite Wall Method if the computing time is the main concern.

Both the Finite Wall and Image Coefficient Methods produced comparable results for the finite thickness single-dielectric or bi-layered sample problem. A comparison of the normalized capacitance values obtained from both methods indicate that they are within 0.7% in all cases.

3.3 FRINGING CAPACITANCE

The dimensions of several standard 50-Ω semi-rigid coaxial lines and the total capacitance of an infinite sample of each of these sensors are given in Table 3. The coaxial line is loaded with teflon ($\varepsilon_r = 2.05$), and water ($\varepsilon_r = 80$) is used as the sample outside the line. These values correspond to the limiting case of a bi-layered medium where the second layer is displaced to infinity.

TABLE 3

Several standard 50-Ω coaxial lines and the total fringe-field capacitance of infinite sample (water).

External Line Dimension [mm]	Nominal b [mm]	Nominal a [mm]	C_T [pF]
6.4 (.25-in)	2.663	0.815	2.5820
3.6 (.141-in)	1.490	0.456	1.4447
2.2 (.085-in)	0.836	0.256	0.8104

Calculations of the fringing capacitance were performed for different positions of the wall until the capacitance value approached that of the infinite sample. Fig. 15 shows the change in capacitance versus distance of the wall in normalized form (valid for any size of 50-Ω teflon-filled sensor), whereas Figs. 16, 17 and 18 show the results in picofarads for the three different standard coaxial lines, i.e. a 6.4-mm line, 3.6-mm line and 2.2-mm line, respectively.

The upper curve in each figure illustrates the capacitance when a metal wall is moved along the axial direction starting from the tip of the sensor (zero millimeters) to a few millimeters away from the sensor, while the lower curve

represents the case for an air wall. The straight line (horizontal) shows the capacitance value with infinite sample. Note that the depth of penetration of the sensor (probe) immersed in the water sample did not affect the capacitance value [28].

Figures 19 to 22 give the percentage difference of sensor capacitance with the wall and the infinite sample as a function of the position of the wall. The results for different sensors commonly used (as given in Table 3) are plotted for convenience.

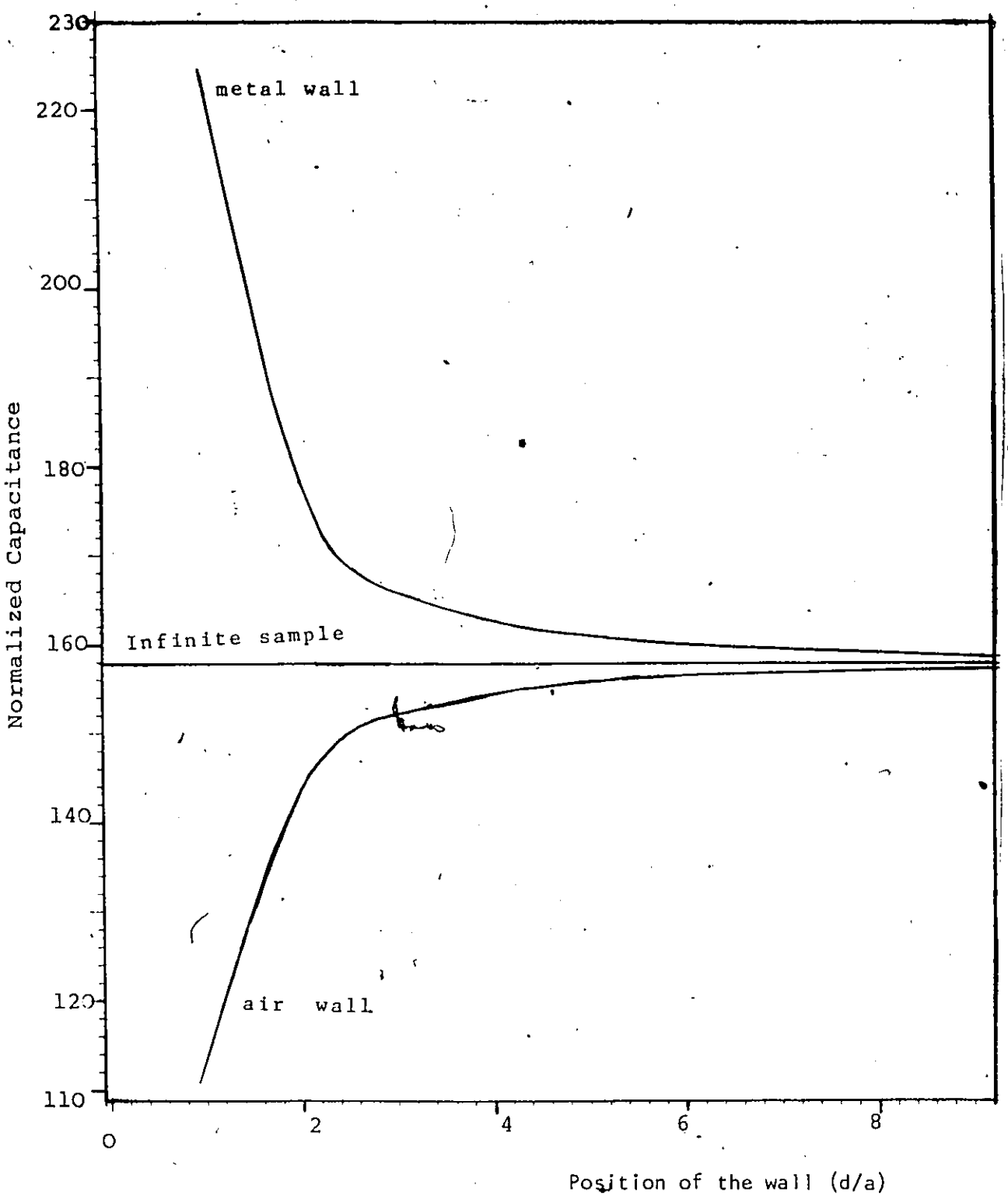

Figure 15: Total capacitance $C_T/\varepsilon_0(b-a)$ versus Displacement of wall d/a for 50-Ω teflon-filled sensors immersed in water.

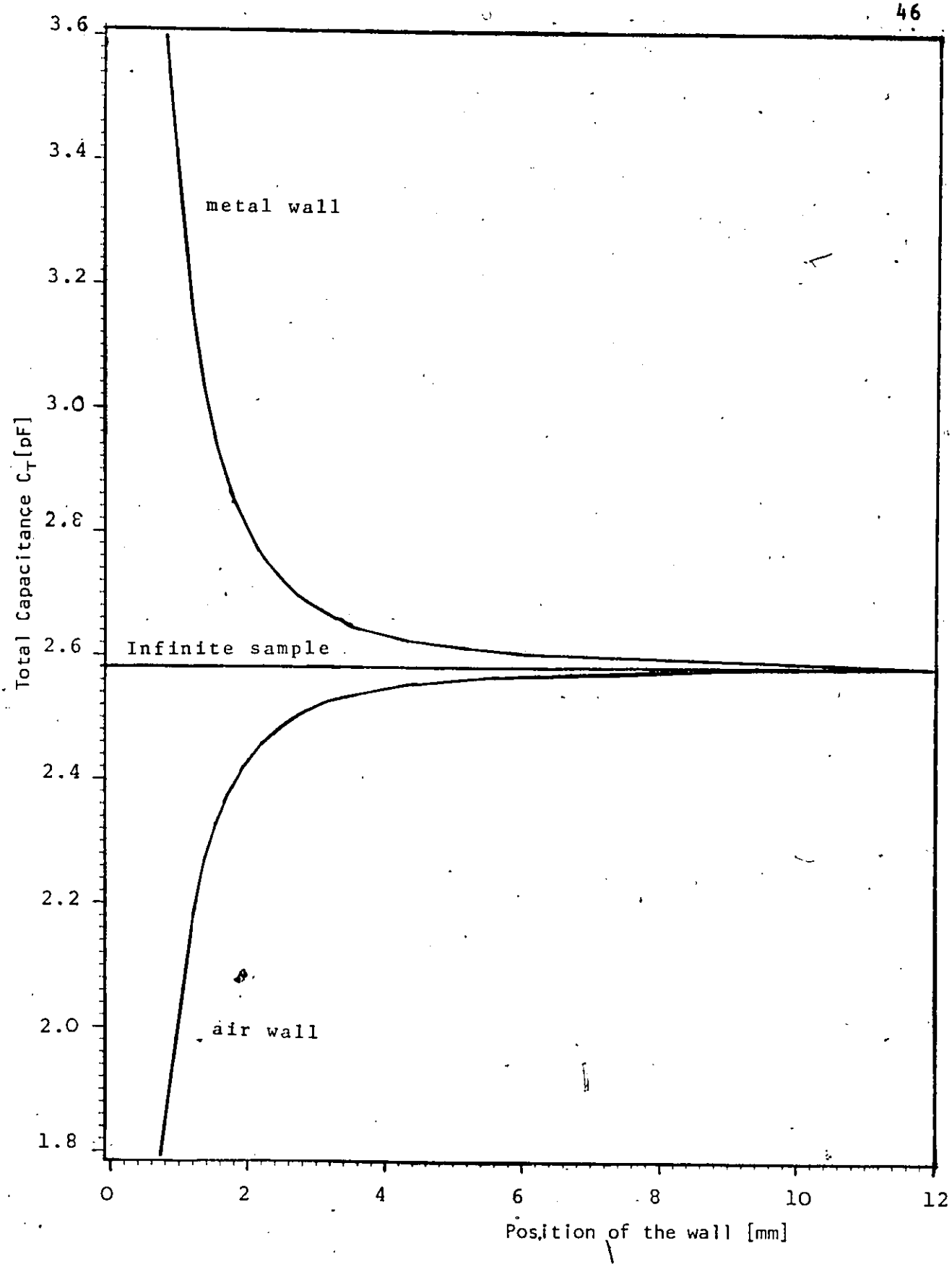

Figure 16: Total capacitance C_T [pF] versus position of the wall d[mm] for a 6.4-mm teflon-line immersed in water.

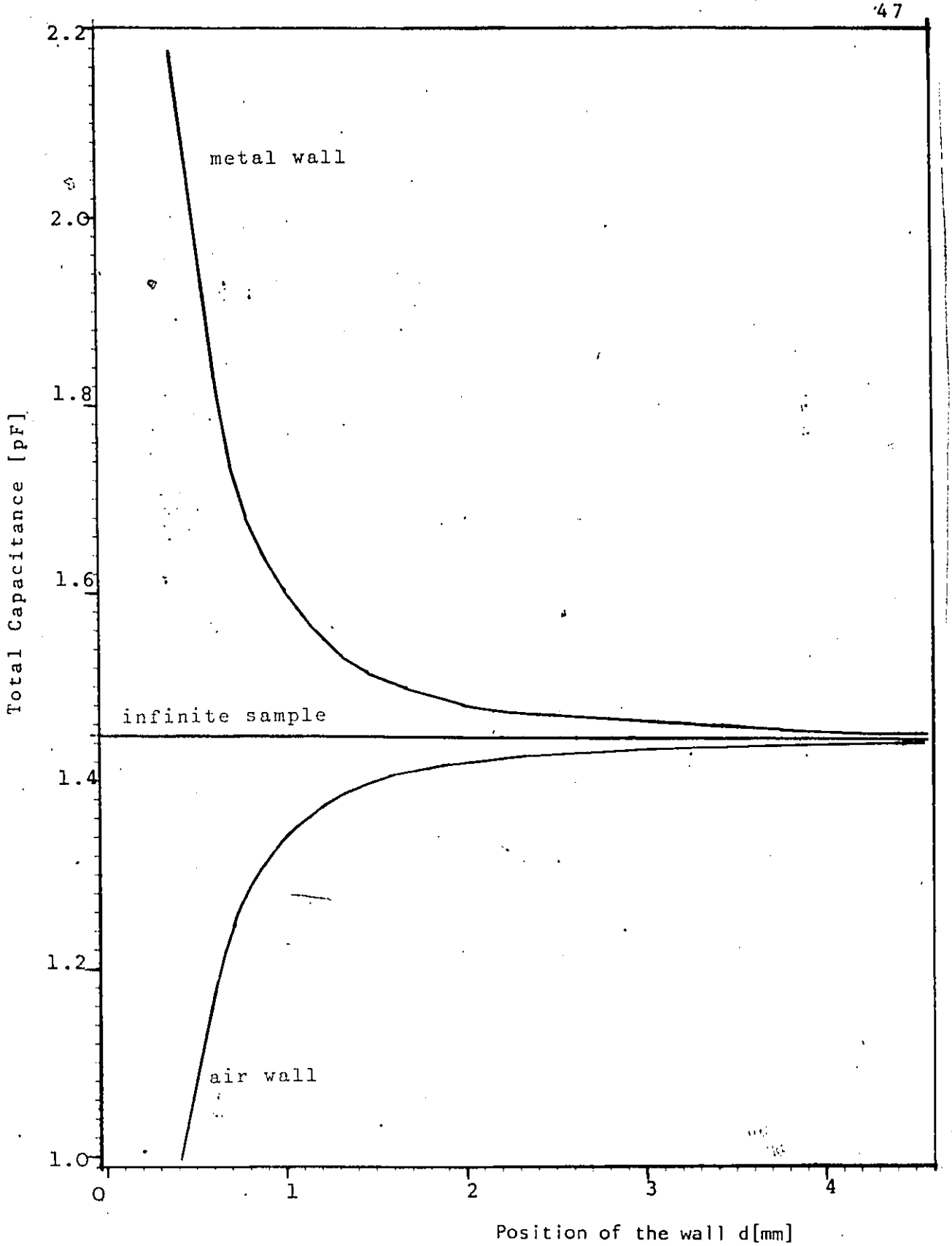

Figure 17: Total capacitance C_T[pF] versus position of the wall d[mm] for a 3.6-mm teflon-line immersed in water.

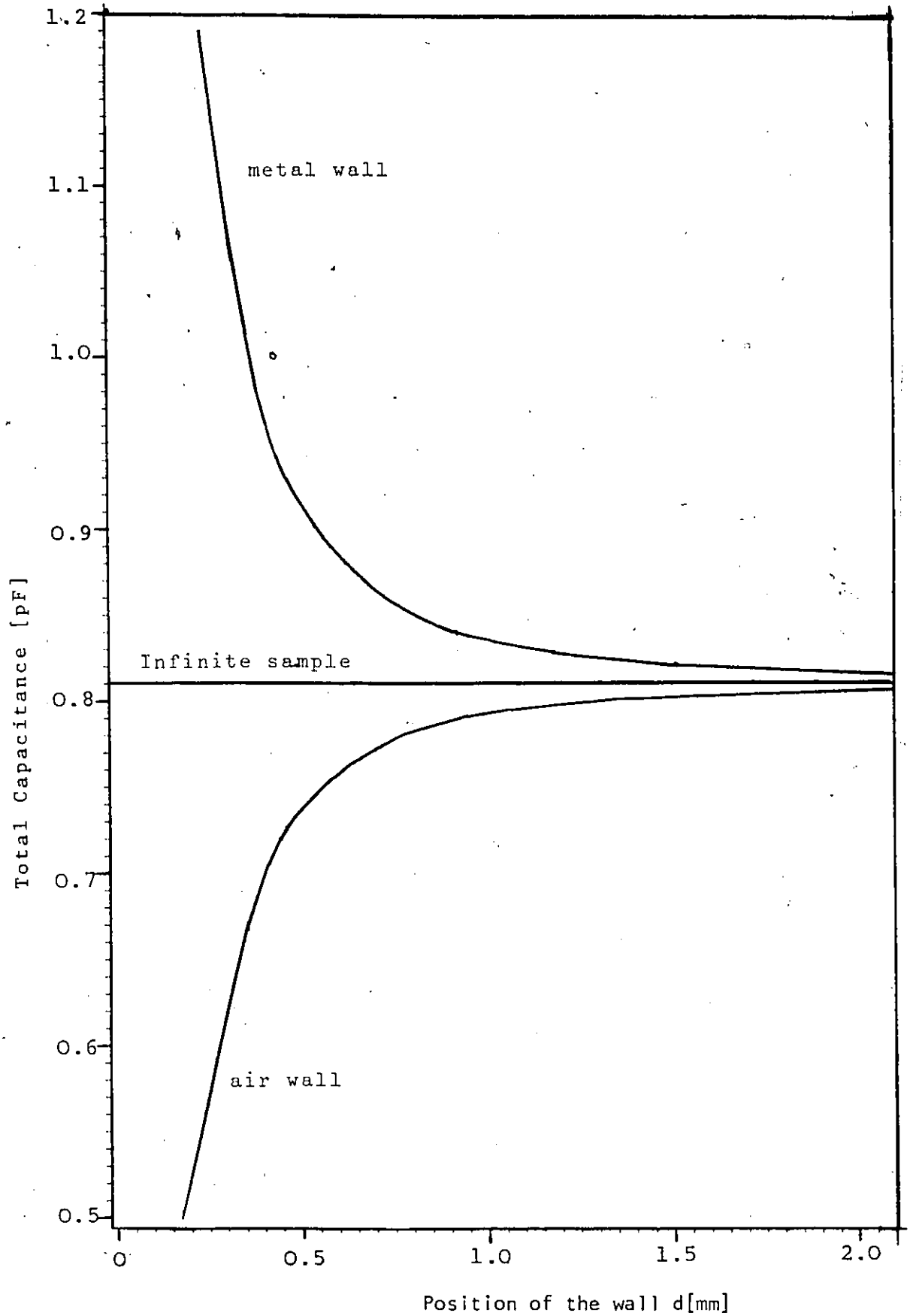

Figure 18: Total capacitance C_T[pF] versus position of the wall d[mm] for a 2.2-mm teflon-line immersed in water.

3.3.1 Discussion

It is evident from Fig. 19 that the capacitance values change rapidly as a metal/air wall moves within a distance of approximately twice the inner-conductance radius from the tip of the sensor (d = 2a). For instance, Figure 20 shows that when the wall is placed at a distance ranging from 2 mm to 6 mm, the change in capacitance is within 1 to 10% for a standard 6.4-mm line. The farther the wall is moved away from the sensor, the smaller the change where it becomes negligible beyond 15 mm. From these data, the minimum sample thickness for simulating an infinite sample may be estimated to be approximately 6 mm of water for a 1% change in capacitance. Since the dielectric constant of water is the limit of permittivities encountered in biological substances at microwave frequencies, the change in capacitance for the latter would be even smaller. Generally, for any teflon-line, a thickness equal to at least seven times the inner radius of the coaxial line sensor is required to simulate an infinite sample.

A summary of the result regarding sensor capacitance differences for the normalized wall position and three standard-sized sensors is given in Table 4. This table provides information on minimum thickness of sample required depending on the desired accuracy.

TABLE 4

Estimation of Sensor Capacitance Difference between finite and infinite sample versus the Position of the Wall.

water $\varepsilon_r = 80$

$\frac{C_{wall} - C_{Inf.}}{C_{Inf.}}$	Position of the Wall: Any sensor normalized to 'a'	6.4-mm dia line	3.6-mm dia line	2.2-mm dia line
%	d/a	d[mm]	d[mm]	d[mm]
> 10%	0 - 2a	0 - 2 mm	0 - 1 mm	0 - .6 mm
1% - 10%	2a - 7a	2 - 6 mm	1 - 3 mm	.6 -1.8 mm
0.1% - 1%	7a -19a	6 -15 mm	3 - 9 mm	1.8 - 5 mm
< 0.1%	> 19a	> 15 mm	> 9 mm	> 5 mm

$C_{Inf.}$ Capacitance with infinite sample.

a = Inner conductor radius of the sensor.

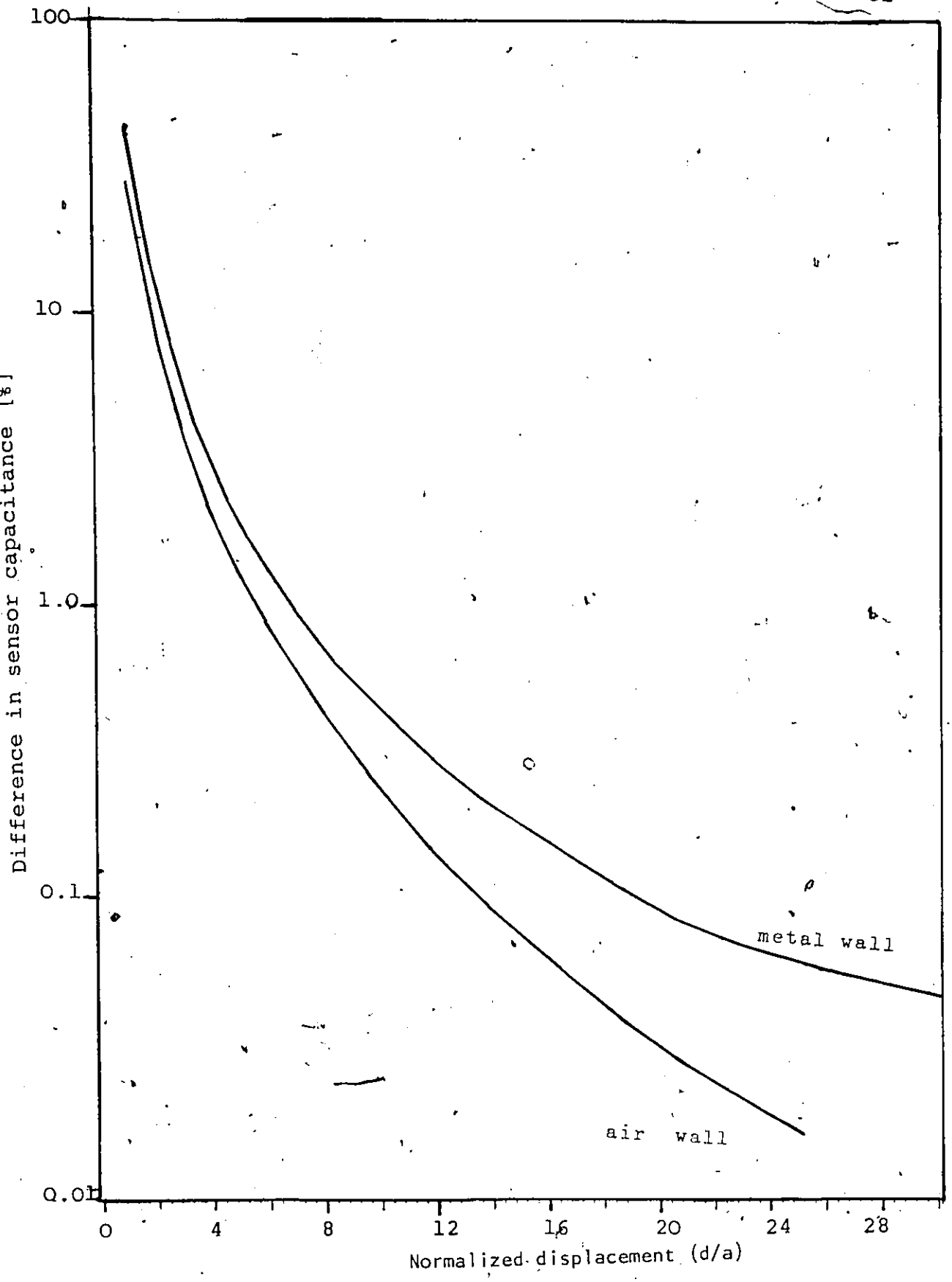

Figure 19: Capacitance difference of the finite thickness and infinite sample vs. the position of wall for 50-Ω teflon-lines.

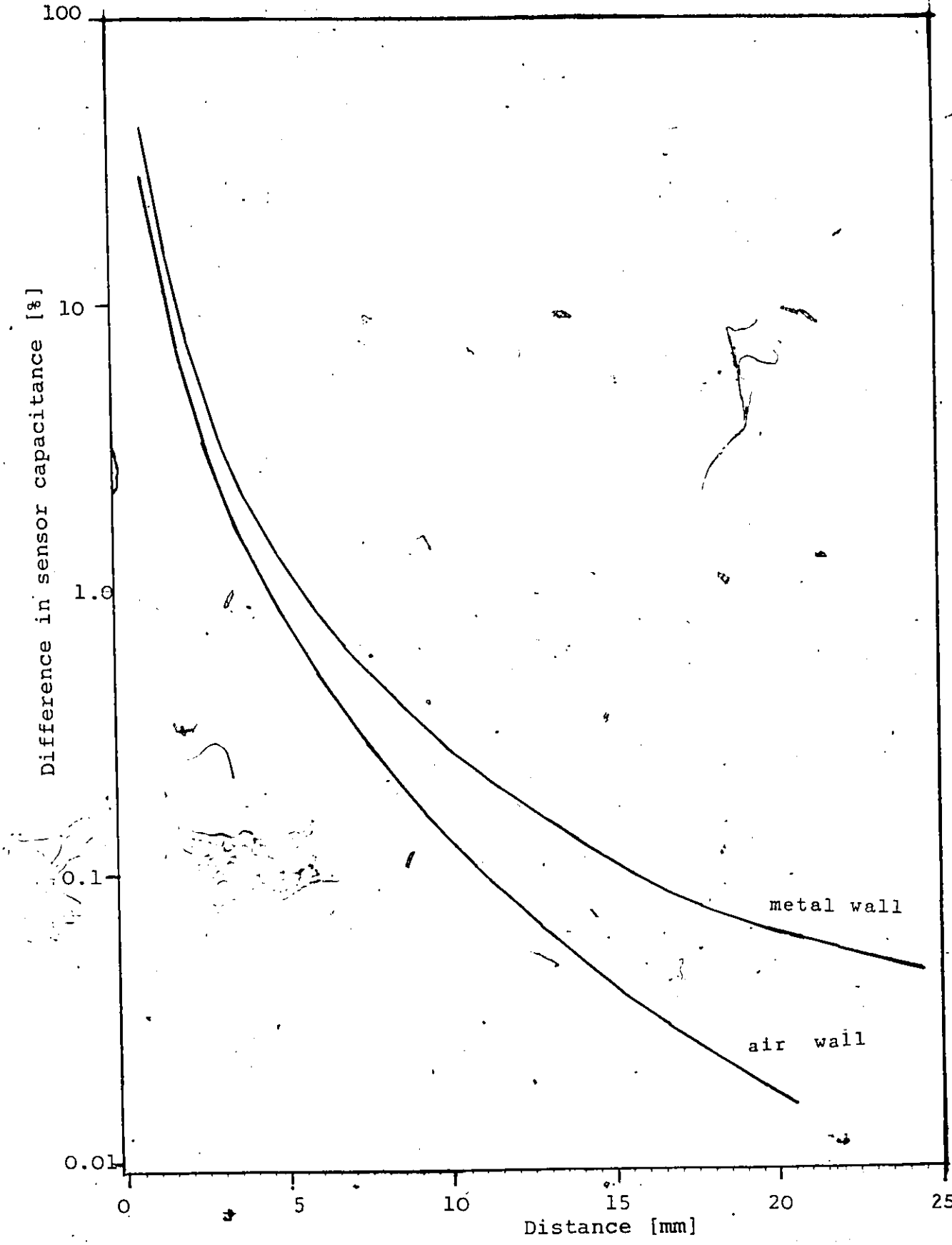

Figure 20: Capacitance difference of the finite thickness and infinite sample versus d [mm] for 6.4-mm sensor.

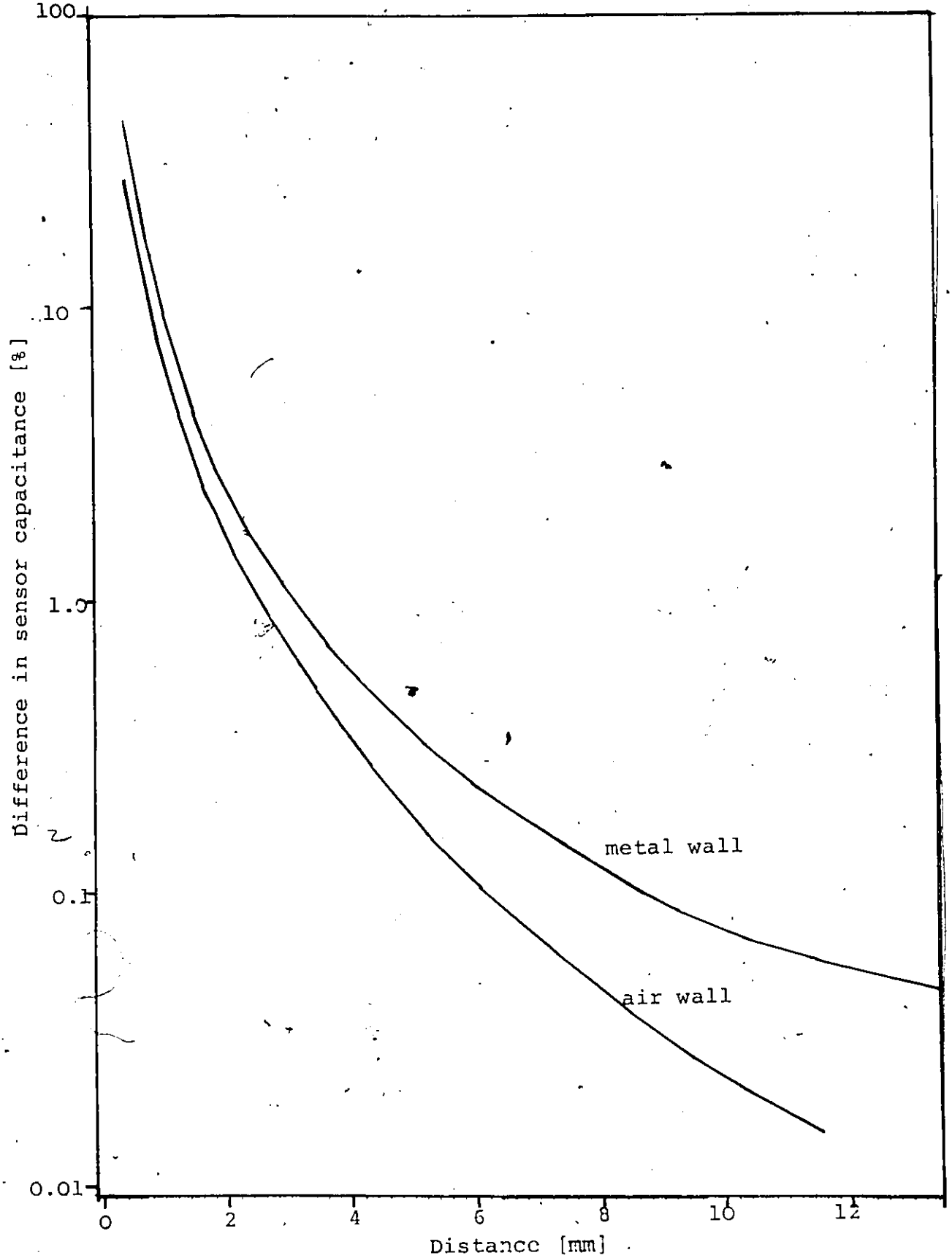

Figure 21: Difference in capacitance of the finite-layer and the infinite sample versus d [mm] for 3.6-mm sensor.

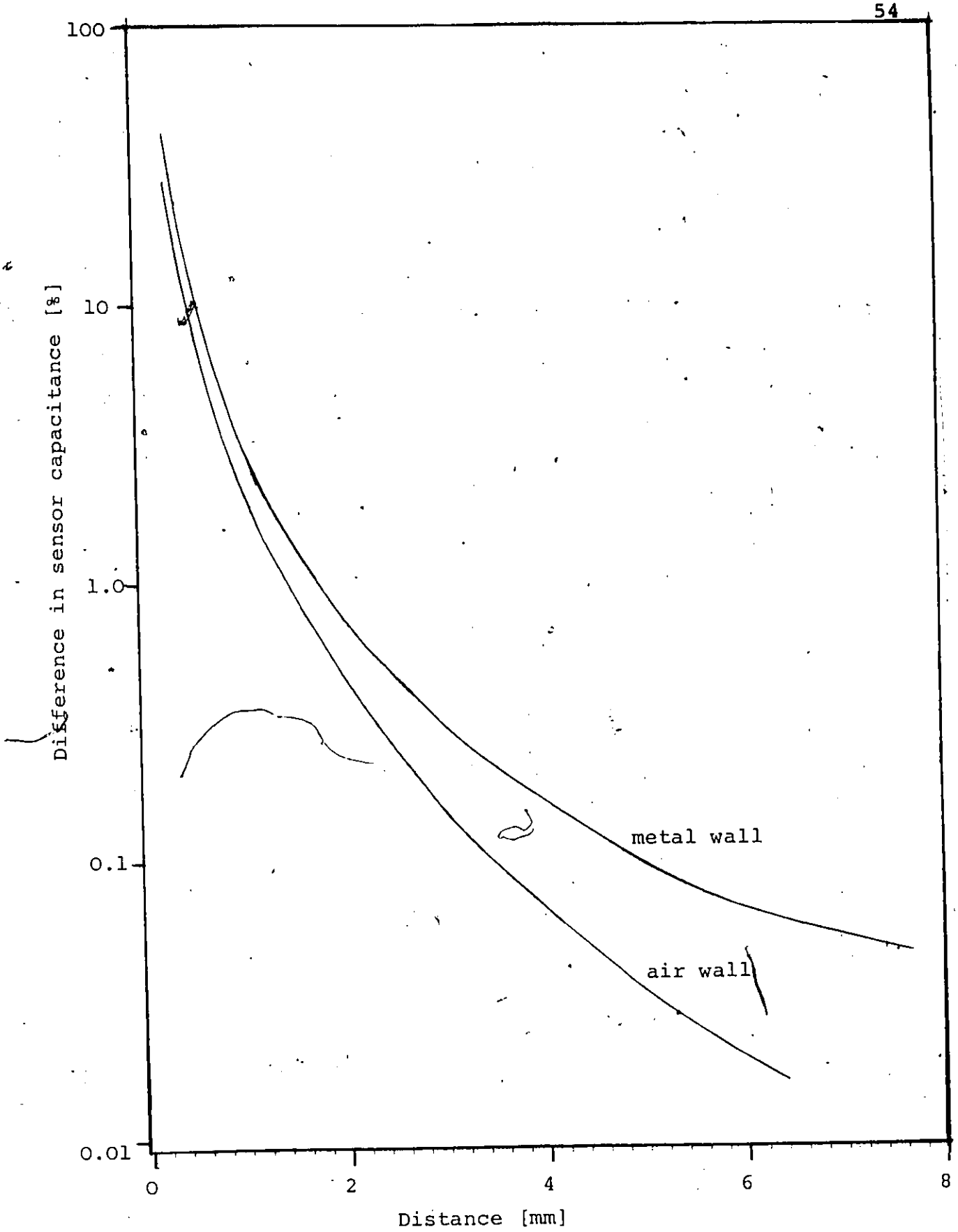

Figure 22: Capacitance difference of the finite-layer and infinite sample versus d [mm] for 2.2-mm sensor.

3.4 ELECTRIC FIELD

The magnitude of the total electric field ($E_T = \sqrt{E_r^2 + E_z^2}$) along a radial line at the aperture of the sensor is calculated using equations (2.31)-(2.33), and plotted in Fig. 23. The field is expressed in volts per unit a where a is the inner conductor radius of the conductor line. It is observed that the maximum field intensity occurs at the radial distance of 1.2 a, while another small peak occurs at approximately 0.98 b (b is the outer conductor inner radius). The ratio of the first and second peak field strengths is approximately 7:1. Beyond the distance c, which is the outer conductor outer radius, the field intensity is negligible. This corresponds to the results in [28], where it was observed that adding a ground plane (metallic flange) to the coaxial line produced insignificant change in the fringing fields and subsequently in the capacitance.

Figure 24 gives the total electric field along a radial line at a distance 'a' from the aperture. The magnitude of the E-field is at maximum around the center conductor and decays with r. The magnitude of the E-field along z-axis is also calculated as shown in Fig. 25(A).

In cases where a bi-layered dielectric sample is used, such as water and air, the total field is mapped as shown in Figs. 25(B) and 26(C). For curve B, the first sample is water ($\varepsilon_r = 80$) with a thickness (distance) of 2 times the inner conductor radius (d = 2a). Beyond this distance the

space is filled with air ($\varepsilon_0 = 1$), and vice versa for curve C where the first sample is air, backed by water.

It is observed from these graphs that the field strength in a high permittivity sample (e.g. water, $\varepsilon_r = 80$) decays much faster than in a low permittivity material (e.g. air, $\varepsilon_0 = 1$) as the distance away from the sensor is increased. A discontinuity in the field occurs at the interface as expected.

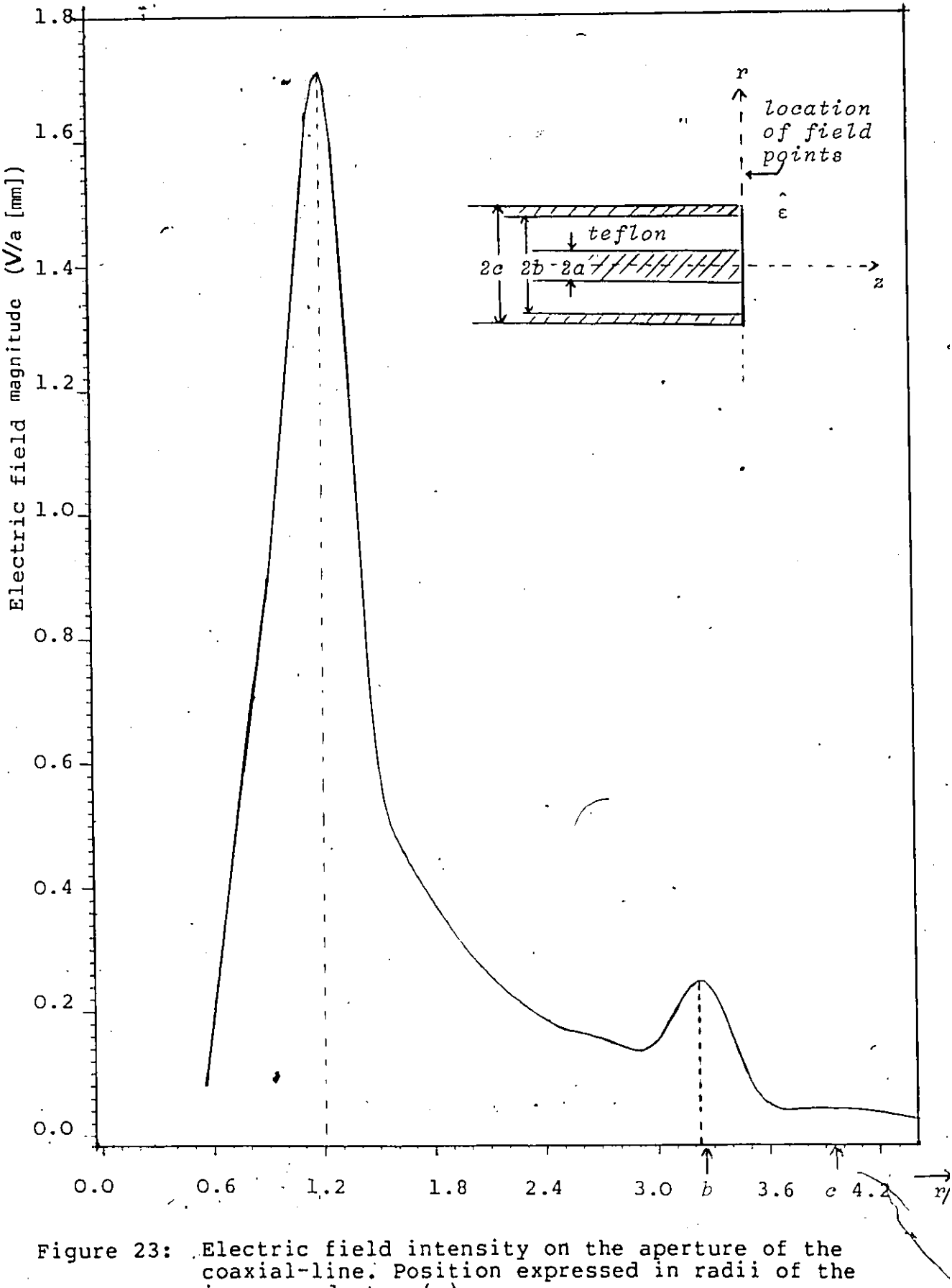

Figure 23: Electric field intensity on the aperture of the coaxial-line. Position expressed in radii of the inner conductor (a).

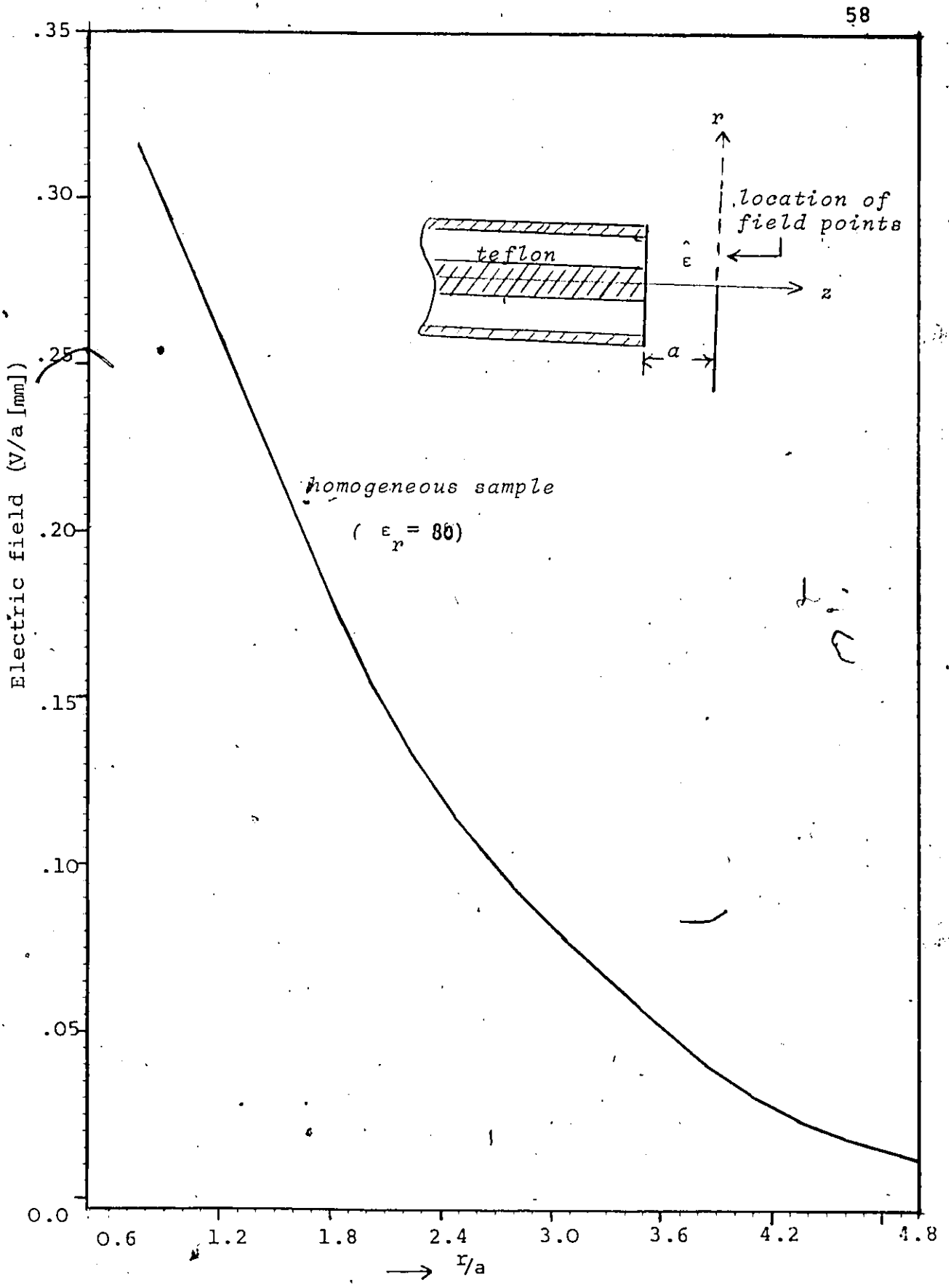

Figure 24: Electric field versus position along the radius. Position expressed in radii of the inner conductor (a).

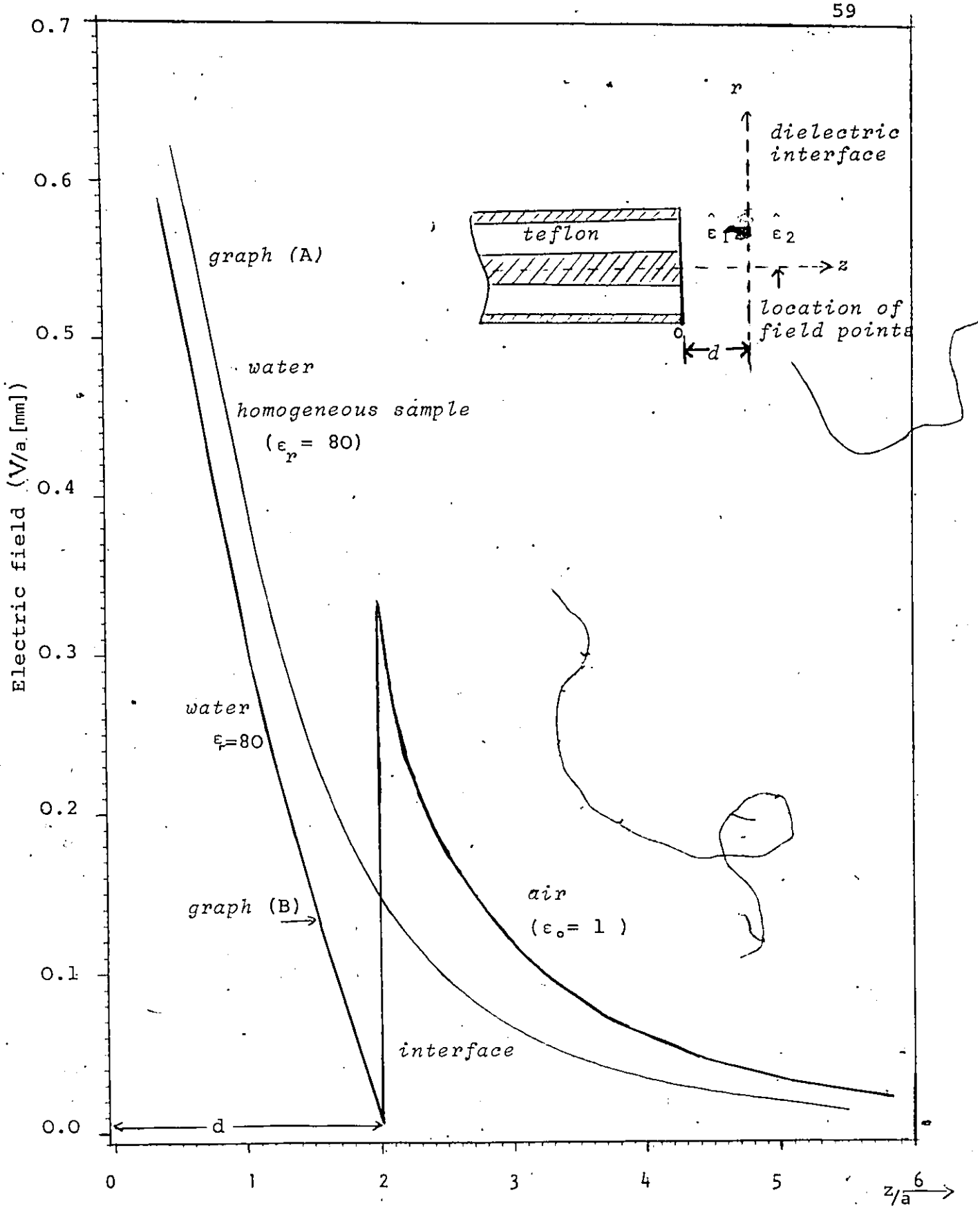

Figure 25: Electric field along the axis. Position expressed in radii of the inner conductor (a).

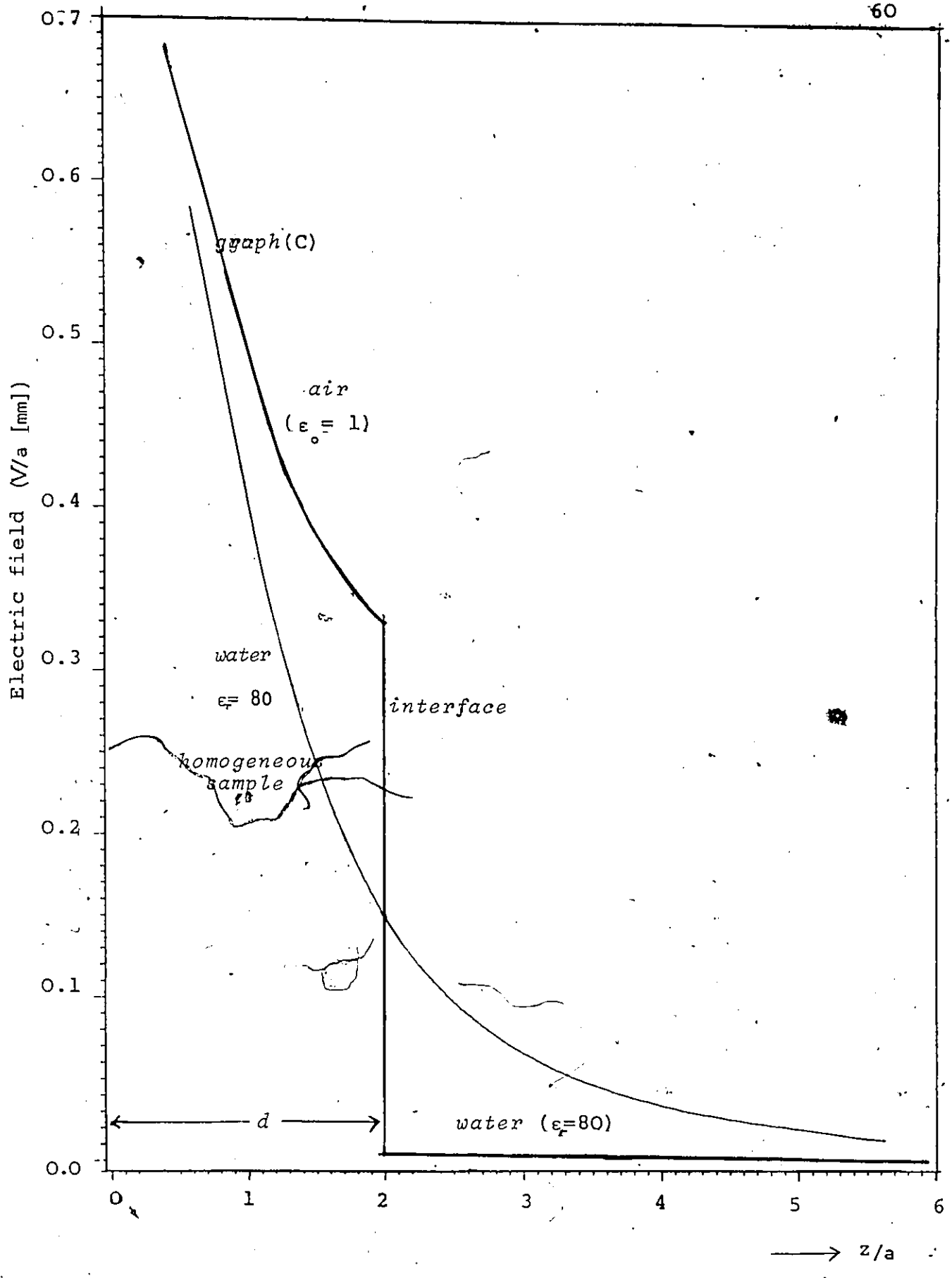

Figure 26: Electric field along the axis. Position expressed in radii of the inner conductor (a).

3.4.1 Discussion

The result in Fig. 23 shows that the most sensitive portion of the sensor with respect to the sample is around the regions of the inner conductor. This result provides useful information for sample preparation and measurement process. It is important to ensure that the sample portion, particularly in the vicinity of high electric field regions, is in good contact with the line. For a semi-solid material, the sample surface should be very flat and smooth to avoid air gaps. For any liquid sample, air bubbles around the open end of the line have to be eliminated before measurements take place.

Figure 24 shows that the field strength at a radial distance 5 times the inner conductor radius ($r = 5a$) is very small. For example, for a 6.4-mm standard line ($a = 0.815$ mm), the magnitude of the electric field is found to be 0.012 V/mm (the potential difference between the inner and outer conductors was set to be equal to 1 V) at a radial position of 4 mm from the center conductor. A similar result is obtained for the case where the distance is along the axial direction (see Fig. 25(A)). The electric field at the axis $z = 5$ mm is found to be 0.020 V/mm (normalized to 1 V between the conductors) for a 6.4-mm line. By knowing the pattern of the electric-field around the sensor, the minimum volume of the sample required in order to prevent reflection from the other closed-by object can be determined. Also,

the depth of the interaction region of the sensor can be evaluated from these results.

Chapter IV

EXPERIMENTAL PROCEDURES AND RESULTS

In this chapter, experimental procedures and results are presented, including a brief description of the equipment used in the measurements, the calibration method and the experimental arrangement.

The measurement method is based on the determination of the input reflection coefficient of an open-ended coaxial line immersed in distilled water backed by either a metal or air wall. With the wall moving in close proximity to the sensor, the input reflection coefficient was measured where its value was used to calculate the total capacitance by assuming a lumped impedance terminating the semi-rigid line.

The experimental results given in this chapter are used to verify the validity of the related numerical methods described in Chapter II. A comparison between the theoretical and the experimental results is presented.

4.1 EQUIPMENT

The key components of the measurement system were the sensor and the computer-controlled Network Analyzer (Hewlett-Packard Model 8410B). The sensor translated changes in the permittivity of a test sample into changes in the input reflection coefficient. The Automated Network Analyzer, operating in the frequency range 0.1-12.4 GHz, was used for fast and accurate measurements of the reflection coefficient.

The measurement system comprised of HP8410B Network Analyzer, HP8745A Test Set, HP8620C RF Signal Source, HP59306A Relay Actuator, HP593134 A/D Converter, HP8656A Synthesized Signal Generator and HP8709A Synchronizer, all controlled by an HP9825A Desktop Computer interfaced through the IEEE-488 interface bus. The block diagram of the system is shown in Fig. 27.

The HP8620C RF Source was programmed to a required frequency for each measurement and combination of linear and polar displays provided accurate magnitude and phase data [34].

The Source Phase-Lock Subsystem consisting of the HP8656A Synthesized Signal Generator and the HP8709A Synchronizer which provided the synthesizer a good frequency accuracy and repeatability. This subsystem provides the frequency accuracy of approximately ± 1 part in 10^6 plus 5 KHz, and frequency repeatability of ± 100 Hz. This accuracy was espe-

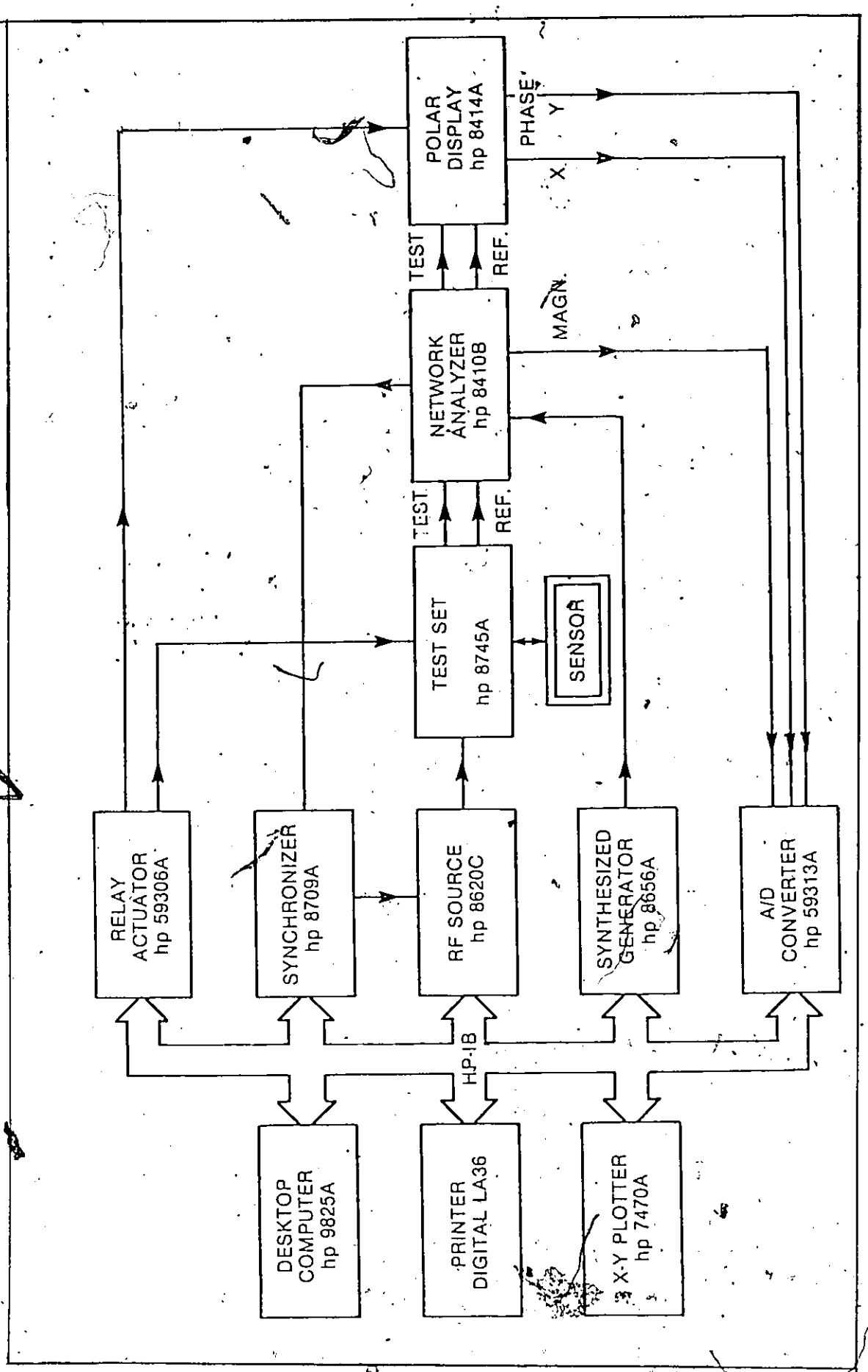

Figure 27: Block diagram of the measuring system.

cially valuable when measuring materials with properties that cause the magnitude or phase to change rapidly with frequency.

4.2 CALIBRATION

One of the most important parts in the measurement procedure was the error correction/calibration of the computer-based automatic network analyzer for the reflection coefficient measurements. To attain high accuracy measurements, the calibration procedure may be performed by using liquids of well known electrical properties (permittivity), namely distilled water, methanol, or saline solution. Water was the most suitable material used as a standard liquid for the system calibration because it was chemically inactive [35,36].

In this calibration procedure, the intrinsic impedance of the liquid used for calibration was calculated and used for calculating the reflection coefficients for the sensor immersed in the same material [37]. The error correcting coefficients were then computed for every frequency on the basis of measured values of the reflection coefficients during calibration and the calculated (known) reflection coefficients of standard terminations or materials. The vector (magnitude and phase) error terms were stored in the computer memory and were used to remove these systematic errors during the measurement procedure as the analyzer tuned back

to each calibration frequency, measured the sensor response and performed the error correction computation. The resulting high-resolution magnitude and phase data of the reflection coefficient were used in the calculations of the other quantity such as the capacitance and transmitted directly to a printer in tabular form.

4.3 EXPERIMENTAL ARRANGEMENT

A typical 6.4-mm (0.25-in) dielectric sensor consisting of an open-ended semi-rigid coaxial line was utilized in the measurements. Distilled water at room temperature (23^{0}C) was chosen as the test dielectric, since it represents the upper limit of the dielectric constant of biological materials at microwave frequencies.

The sensor was immersed in a container filled with distilled water mounted on a moveable carriage. A metal wall was achieved by placing a metallic plate at the bottom of the container while an air wall was simulated using a sheet of styrofoam which had a thickness of 2 cm. The height of the open end of the sensor above the wall was measured using a dial gauge as shown in Fig. 28.

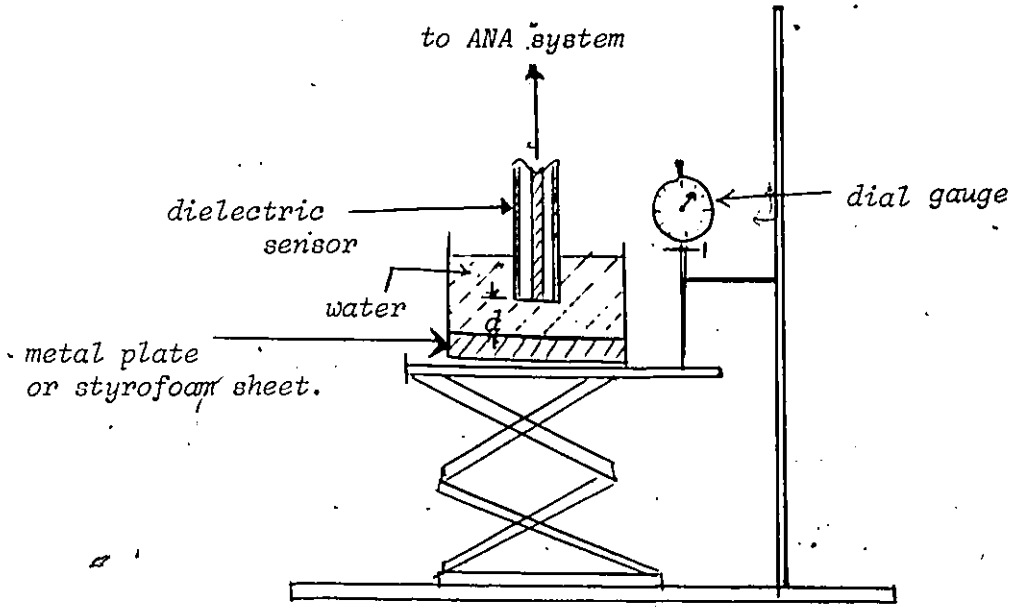

Figure 28: Experimental arrangement.

4.4 MEASUREMENT PROCEDURES

The system was allowed to warm up for several hours prior to taking the measurements. The programs were then loaded into the HP9825A computer and calibration was done with an open circuit, distilled water and a saline solution.

It is important to ensure that no air bubbles exist at the open end of the sensor since a minute pocket of air may cause large errors. The frequency range was selected from 0.2 GHz to 2.0 GHz with an incremental step of 100 MHz, because it was shown in [35] that the change in the fringe-field capacitance with frequency is negligible in this fre-

quency range. This criterion can be justified by using the following empirical formula [35]:

$$C_T = C_{T'}\left(1 + \frac{F^2}{24}\right) \quad [pF] \tag{4.3}$$

where

$$F = 2\pi f\,(b - a)\,\varepsilon_0\sqrt{\varepsilon_r} \tag{4.4}$$

where a and b are the internal and external radii of the line, respectively, ε_0 is the dielectric constant of free space (air) and ε_r is the dielectric constant of the material filling the line ($\varepsilon_{Tef.} = 2.05$), and $C_{T'}$ is the static value of the fringe-field capacitance of water. Using this expression (4.3), the frequency correction of the open-circuited capacitance for various types of teflon-filled coaxial lines immersed in water can be calculated:

1. For 2.2-mm line: $C_T(f) = 0.8104 + 1.454\ f^2 * 10^{-10}$ [pF]
2. For 3.6-mm line: $C_T(f) = 1.4447 + 4.08\ f^2 * 10^{-10}$ [pF]
3. For 6.4-mm line: $C_T(f) = 2.5820 + 2.33\ f^2 * 10^{-9}$ [pF]

where f is the frequency in megahertz. For frequency ranging from 0.2 GHz to 2 GHz, the maximum error due to frequency correction is 0.07% for 2.2-mm line, 0.1% for 3.6-mm line and 0.36% for 6.4-mm line.

Measurements of an infinite sample was first made by immersing the sensor in a large (150-ml beaker) container of water without interference of any close by objects (e.g. wall). A metallic plate or styrofoam sheet was then moved closer at each measurement to the sensor and the distance

between the tip of the sensor and the wall was determined by using a dial gauge (see Fig. 28). Once the values of the input reflection coefficient were measured and known, they were used to calculate the total fringe-field capacitance of the sensor using the following equation (see section 1.3, equations (1.1)-(1.3)):

$$C_T = \frac{(1 - S_{11} e^{j\phi_{11}})}{j\omega z_0 (1 + S_{11} e^{j\phi_{11}})} \qquad (4.5)$$

Measurements were performed at different distances of the sensor above the wall thus producing a set of values of total capacitance as a function of the wall position. These procedures were then repeated ten times where the average (mean) values were obtained and were used to compare with the theoretical results.

4.5 ERROR ANALYSIS

The errors which occur in this measurement can be divided into two categories, i.e., systematic errors, which are repeatable and can be measured and corrected by the system through calibration, and nonsystematic errors, which are random error (not repeatable). The latter includes the discontinuities introduced by connectors and other physical changes in the test setup between calibrations and measurements. The most common errors are due to the following factors:

1. Imperfect contact with the test sample such as formation of a small air bubble in water sample.
2. Temperature drift, particularly due to changes in the length of the coaxial line connectors. This problem can be reduced by warming up the measurement system before the tests were performed.
3. Imperfect connections during calibrations may cause large correction parameters. This problem should be corrected before proceeding to further measurements.
4. Lack of repeatability of connections, noise or other unknown causes could also cause error in the measurements. Repeating the calibration procedure was necessary in this case.

Fortunately, the effects of all these errors can be reduced if the experimental measurements are proceeded with care and a proper calibration is done.

4.6 EXPERIMENTAL RESULTS

The values of the measured capacitance C_T [pF] versus the wall position d [mm] is plotted in Fig. 29 and compared with the theoretical result.

TABLE 5

Experimental values of the capacitance [pF] versus the position of the wall [mm] for a 6.4-mm teflon line.

ε_r = 80 (water)
T = + 23 °C

	Metal Wall			Air Wall		
d [mm]	Average C_T [pF]	Standard Deviation		Average C_T [pF]	Standard Deviation	
1.0	2.220	0.083	2.6%	2.139	0.026	1.2%
2.0	2.730	0.048	1.7%	2.440	0.023	0.9%
3.0	2.625	0.053	2.0%	2.518	0.021	0.8%
4.0	2.593	0.042	1.6%	2.546	0.028	1.1%
6.0	2.576	0.036	1.4%	2.561	0.035	1.4%
8.0	2.573	0.030	1.2%	2.577	0.026	1.0%
10.0	2.578	0.025	0.9%	2.580	0.025	0.9%

Note that the values of C_T, indicated in Table 5 are mean values averaged over all the measurements taken at a fixed position of the wall. The straight line shown in Fig. 29 represents the total capacitance value with infinite sample

(no wall) which is equal to 2.582 pF. The solid lines (curves) represent calculated values from numerical methods while square points indicate experimental results. Vertical bars indicate the standard deviations of ten repeated measurements at any given point, where the standard deviations describe the reproducibility of the results.

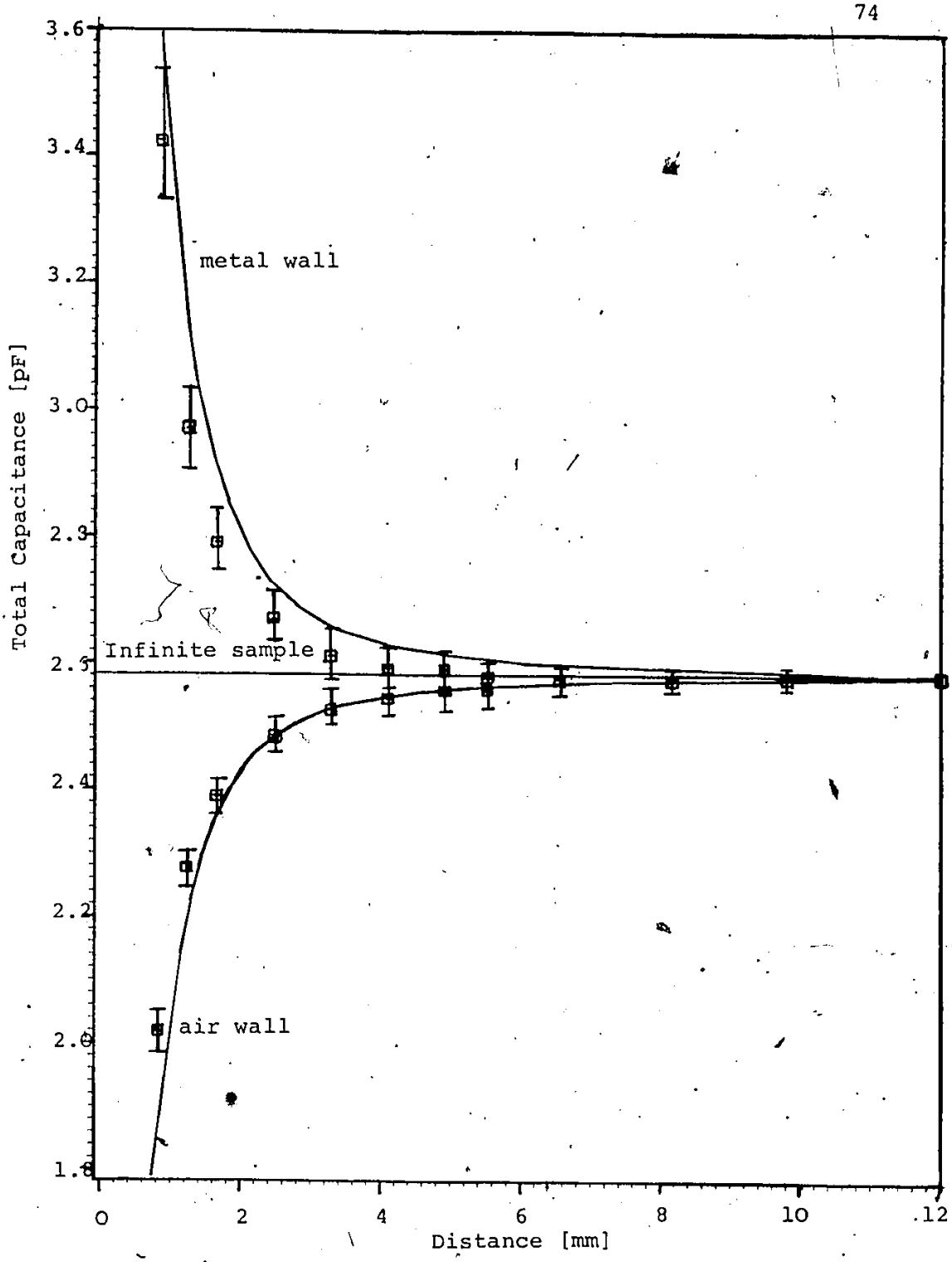

Figure 29: Comparison of the experimental results with the theoretical ones.

4.7 COMPARISON BETWEEN NUMERICAL AND MEASURED RESULTS

The experimental results agree very well with the theoretical values obtained from either the Image Coefficient Method or Finite Wall Method. Larger values of standard deviation occured at distances below 5 mm. This is due to the rapid changes of the sensor capacitance when the wall is brought close to the sensor. For instance, when two parallel conducting plates are brought closer to each other, the value of the capacitance will increase as the distance of wall decreases. In the experiments, it was difficult to set the distance accurately even though a precision dial gauge was used. However, for the majority of experimental points, the deviation from the mean value was less than 2% as shown in Table 5.

Chapter V

SUMMARY AND CONCLUSION

In this chapter, a summary of this thesis is given. Also, some suggestions for the future research and development are presented.

5.1 SUMMARY

Chapter I gave a review of several methods used by reseachers in measurements of dielectric properties and a variety of sample holders with their sample configurations were given. The equivalent lumped-circuit of the sensor, which represents a linear-model relationship between the sample permittivity and the static fringe-field capacitance of the sensor was presented. It yields closed-form expressions for the permittivity as a function of the measured input reflection coefficient.

Chapter II gave a brief review of static conductor-dielectric problems and the Moment Method used in their solution. Two approaches were used to account for the presence of the conducting or dielectric wall. They were the Finite Wall Method and the Image Method. In the first method, the wall which was assumed to have finite area, was subsectioned in a manner similar to the other conductors and interfaces.

In the later method, the infinite conducting or dielectric wall was replaced by an infinite series of image charges. Both were implemented using a digital computer.

Chapter III presented the numerical results. The fringe-field capacitance calculated by the Finite Wall Method and the Image Coefficient Method was compared. The minimum sample thickness required to simulate an infinite sample was estimated from the results. The total dielectric field distribution along radial and axial lines from the aperture were plotted for both homogeneous and inhomogeneous dielectric samples.

Chapter IV described the experimental procedures and the equipments used. The error analysis was also discussed. The computer program for permittivity measurements using the open-ended coaxial line sensor and the automated network analyzer was written in HPL language and is given in Appendix B. Finally, the measured value of the capacitance was presented. The comparison between the theoretical (numerical) and experimental results showed good agreement.

5.1.1 Future Research

An interesting extension of this work would be to replace the bi-layered sample with a multi-layer dielectric sample such as biological tissue. Using the Finite Wall Method, an additional wall which simulates the interface of the second and third layers may be solved likewise for the bi-layered sample shown in this thesis. The multi-layer problem would be more complicated using the Method of Images because of the multiple reflections due to the second interface. It is expected to produce a more complicated Green's function, therefore, considerably increasing the CPU time. In addition, it would be interesting to analyse the case of lossy media, e.g. biological substances, where the loss factor can not be neglected and must be included in the analysis.

5.2 CONCLUSIONS

In this thesis the configuration of an open-ended coaxial line in contact with a finite thickness sample has been analysed, in order to evaluate the response of the sensor when utilized to measure the properties of inhomogeneous dielectrics. Also, the minimum sample thickness for simulating an infinite sample has been estimated.

The Method of Moments was used to solve the static conductor-dielectric problem and two separate approaches were used to account for the presence of the bi-layered medium in the solution. The numerical results were verified experi-

mentally by measuring the fringing capacitance of the sensor in a bi-layered medium.

The numerical results agreed very well with the experiment. The required thickness of the sample depends on the size of the sensor used in measurements. For example, for a standard 6.4-mm line, a water sample of at least 6 mm thickness may be regarded as an infinite sample within only 1% error.

The accomplishments achieved in this study are as follows:

1. Two separate numerical approaches have been used to investigate the effects of a wall, simulating an inhomogeneous dielectric sample;
2. The preparation and implementation of the computer programs for these two methods were presented;
3. The minimum sample thickness for simulating an infinite sample has been estimated;
4. The numerical results were verified by the experimental values using an automated network analyzer and they were found to be in good agreement;
5. The electric field patterns were mapped along radial and axial lines at the aperture. The region of the highest electric field was found to be in the vicinity of the center conductor.

Appendix A

FORTRAN PROGRAM: METHOD OF MOMENTS

The listings of the computer programs used in this work are given. Appendix A.1 gives a listing of the Method of Moments program where the wall is solved by the finite wall approach. Since the program for the Method of Images utilizes the same as in Appendix A.1, except for the subroutine of the Green's function which replace the subsections of the wall, only the subroutine GREEN is reproduced in Appendix A.2.

A.1 PROGRAM LISTINGS OF THE FINITE WALL METHOD

```
C     ****************************************************************
C     *  Program name: FNWALL                                        *
C     *                                                              *
C     *  Purpose: To calculate the coaxial-line capacitance          *
C     *           and the electric-field in a bi-layer               *
C     *           dielectric sample.                                 *
C     *                                                              *
C     *  Method:  Finite Wall Method                                 *
C     ****************************************************************
C
C
      IMPLICIT REAL*8 (A-H,O-Z)
      REAL*8 K(89,89),R(89),Z(89),RI1(89),RI2(89),ZI1(89),ZI2(89),
     &POT(89),CHECK(10),C(10,89),AINV(89,89),WKAREA(8188),Q(89),
     &RS(10),ZS(10),DELP(20),DELR(10),DELZ(10),ER(10),EZ(10)
C
        INTEGER PR
C
C     Coordinates ( RI1(I),ZI1(I) ) and ( RI2(I),ZI2(I) )
C     represent the end point of the "I" th charge pulse.
C     Number the charge pulses beginning with the pulses
C     being held at a potential of 1 volt.
C
C     Subsectional points on the coaxial line and the wall:
C
        DATA RI1/15*1.0,1.0,.95,.9,.8,.7,.6,.5,.35,.2,
     &15*3.268,3.268,3.3,3.35,3.45,3.55,3.65,3.75,3.85,
     &11*3.925,0.0,.5,1.0,1.5,2.0,2.5,3.0,3.5,4.0,4.5,5.0,5.5,
     &6.0,6.5,1.0,1.05,1.15,1.25,1.4,1.6,2.0,2.4,2.6,2.8,2.9,
     &2.95,3.0,3.05,3.1,3.15,3.2/
C
        DATA RI2/15*1.0,.95,.9,.8,.7,.6,.5,.35,.2,0.0,
     &15*3.268,3.3,3.35,3.45,3.55,3.65,3.75,3.85,3.925,
     &11*3.925,.5,1.0,1.5,2.0,2.5,3.0,3.5,4.0,4.5,5.0,5.5,
     &6.0,6.5,7.0,1.05,1.15,1.25,1.4,1.6,2.0,2.4,2.6,2.8,
     &2.9,2.95,3.0,3.05,3.1,3.15,3.2,3.268/
C
        DATA ZI1/0.0,.5,1.0,1.5,2.0,2.4,2.8,3.1,3.3,3.5,
     &3.6,3.7,3.8,3.9,3.95,9*4.0,0.0,.5,1.0,1.5,2.0,2.4,
     &2.8,3.1,3.3,3.5,3.6,3.7,3.8,3.9,3.95,8*4.0,4.0,3.9,
     &3.8,3.7,3.5,3.3,3.0,2.7,2.3,1.6,.9,14*6.0,17*4.0/
C
        DATA ZI2/.5,1.0,1.5,2.0,2.4,2.8,3.1,3.3,3.5,3.6,
     &3.7,3.8,3.9,3.95,4.0,9*4.0,.5,1.0,1.5,2.0,2.4,2.8,
     &3.1,3.3,3.5,3.6,3.7,3.8,3.9,3.95,4.0,8*4.0,3.9,
     &3.8,3.7,3.5,3.3,3.0,2.7,2.3,1.6,.9,0.0,14*6.0,17*4.0/
```

```
C
C     The field points along the radial displacements:
C
      DATA RS/.25,.5,.75,1.0,1.25,1.5,1.75,2.0,2.25,2.5/
      DATA ZS/10*6.0/
C
C     POT(I) represents the value of potential for pulse I.
      DATA POT/24*1.0D0,65*0.0D0/
C
C     NPULT - Total No. of pulses including interface.
C     NDPUL - Number of pulses lying on conductors.
C     NUNI - Number of pulses being held at 1 volt.
      NPULT=89
      NDPUL=58
      NUNI=24
      NIN=15
C
C     EPS4 - The dielectric constant of the second layer sample (air).
C     EPS3 - The dielectric constant of the first layer sample (water).
C     EPS2 - The dielectric constant inside the line (teflon).
      EPS2=2.05D0
      EPS3=80.0D0
      EPS4=1.0D0
C
C     SCALE - Scale factor for all dimensions.
      SCALE=1.0D0
C
C
C     If PR = 1, do not print charge densities.
      PR=0
C     Scaling of the dimensions:
      DO 87 I=1,NPULT
      RI1(I)=RI1(I)*SCALE
      RI2(I)=RI2(I)*SCALE
      ZI1(I)=ZI1(I)*SCALE
      ZI2(I)=ZI2(I)*SCALE
   87 CONTINUE
C
C     Calculation of coordinates of pulse centres:
      DO 1 I=1,NPULT
      R(I)=(RI1(I)+RI2(I))/2.0D0
      Z(I)=(ZI1(I)+ZI2(I))/2.0D0
    1 CONTINUE
C
C     Using numerical integration to construct the upper system:
C     Set KCODE equal to 1 for regular Green's function kernel,
      KCODE=1
C
      DO 2 I=1,NDPUL
      DO 3 J=1,NPULT
      IF((I.EQ.J).AND.(RI1(J).EQ.RI2(J))) GOTO 50
      CALL GAUSS(R(I),Z(I),RI1(J),RI2(J),ZI1(J),ZI2(J),SUM,KCODE)
      GOTO 51
   50 CALL DIRZ(R(I),Z(I),R(J),ZI1(J),ZI2(J),SUM)
C
```

```
C     Calculation of the "IMAGE" element:
   51 CALL GAUSS(R(I),Z(I),RI1(J),RI2(J),-ZI1(J),-ZI2(J),SMP,KCODE)
      K(I,J)=SUM+SMP
    3 CONTINUE
    2 CONTINUE
C
C     Calculation of the lower system:
      NNN=NDPUL+1
C
      DO 32 I=NNN,NPULT
C     Set KCODE depending on orientation of 'I'th element:
      KCODE=2
      IF(RI1(I).EQ.RI2(I)) KCODE=3
C
      DO 33 J=1,NPULT
      CALL GAUSS(R(I),Z(I),RI1(J),RI2(J),ZI1(J),ZI2(J),SUM,KCODE)
C     Calculation of the "IMAGE" element:
      CALL GAUSS(R(I),Z(I),RI1(J),RI2(J),-ZI1(J),-ZI2(J),SMP,KCODE)
      IF(I.GT.72) GOTO 34
      K(I,J)=(SUM+SMP)*(EPS4-EPS3)
      IF(I.EQ.J) K(I,J)=K(I,J)-(EPS4+EPS3)/2.0D0
      GOTO 33
   34 K(I,J)=(SUM+SMP)*(EPS3-EPS2)
      IF(I.EQ.J) K(I,J)=K(I,J)-(EPS3+EPS2)/2.0D0
   33 CONTINUE
   32 CONTINUE
C
C     Solve the system for the charge pulse heights:
C     ----------------------------------------------
C     LINV2F - IMSL subroutine name.
C     K - Input matrix of dimension N by N containing
C         the matrix to be inverted.
C     IA - Row dimension of the matrix.
C     AINV - Output matrix of dimension N by N containing
C            the inverse of K.
C     IDGT - Input option.
C     WKAREA - Work area of dimension equal to N**2+3N.
C     IER - Error parameter (output).
      N=NPULT
      IA=NPULT
      IDGT=4
      CALL LINV2F(K,N,IA,AINV,IDGT,WKAREA,IER)
      DO 554 I=1,NPULT
      Q(I)=0.0D0
  554 CONTINUE
      DO 555 I=1,NPULT
      DO 556 J=1,NPULT
  556 Q(I)=Q(I)+AINV(I,J)*POT(J)
  555 CONTINUE
C
```

```
C     Calculate the total electric field along the radial displacement:
C     ----------------------------------------------------------------
      WRITE(6,66)
   66 FORMAT(2X,'THE ELECTRIC FIELD ALONG THE RADIAL DISTANCE')
C
      DO 11 I=1,10
      CHECK(I)=0.0D0
   11 CONTINUE
C
      KCODE=1
      DO 12 I=1,10
      DO 13 J=1,NPULT
      CALL GAUSS(RS(I),ZS(I),RI1(J),RI2(J),ZI1(J),ZI2(J),SM,KCODE)
      CALL GAUSS(RS(I),ZS(I),RI1(J),RI2(J),-ZI1(J),-ZI2(J),SP,KCODE)
      C(I,J)=SM+SP
      CHECK(I)=CHECK(I)+C(I,J)*Q(J)
   13 CONTINUE
      IF(I.EQ.1.OR.I.EQ.10) GOTO 88
      N=I-1
      DELP(I)=DABS(CHECK(N)-CHECK(I))
      DELR(I)=RS(I)-RS(N)
      ER(I)=DELP(I)/DELR(I)
   88 WRITE(6,77)I,RS(I),ZS(I),CHECK(I),ER(I)
  332 CONTINUE
   77 FORMAT(1X,'I= ',I2,2X,'RS= ',F4.2,2X,'ZS= ',F4.2,2X,
     &'POT= ',F7.4,2X,'ER= ',F7.4)
   77 FORMAT(8X,I2,5X,F7.4)
   12 CONTINUE
C
C
C     OUTPUT SECTION:
C     ---------------
  119 WRITE(6,100)NPULT
  100 FORMAT(1X,' TOTAL NUMBER OF PULSES: NPULT=',I5)
      WRITE(6,107) NDPUL
  107 FORMAT(1X,'NO. OF DIRICHLET PULSES: NDPUL =',I5)
      IF(PR.EQ.1) GOTO 305
      WRITE(6,101)
  101 FORMAT(1X,'PULSE NO.  R-COORD.  Z-COORD.  CHARGE DENSITY')
      WRITE(6,102)(I,R(I),Z(I),Q(I),I=1,NDPUL)
  102 FORMAT(1X,I4,2X,F8.4,2X,F8.4,2X,D17.7)
      WRITE(6,122)
      NDIEL=NPULT-NDPUL
      WRITE(6,108) NDIEL
  108 FORMAT(1X,'NO. OF DIEL-DIEL BDRY PULSES: NDIEL =',I5)
      WRITE(6,102)(I,R(I),Z(I),Q(I),I=NNN,NPULT)
  305 WRITE(6,122)
      WRITE(6,351) EPS2,EPS3,EPS4
  351 FORMAT(1X,'EPS2 = ',F4.2,' EPS3 = ',F8.4,2X,' EPS LAYER=',F8.4)
C
```

```
C     CALCULATION OF THE TOTAL CHARGE AND CAPACITANCE:
C     ------------------------------------------------
      CAPOUT=0.0D0
      CAPIN=0.0D0
C     CALCULATION OF FREE CHARGE
      DO 5 I=1,NUNI
      CHAR=Q(I)*R(I)*DSQRT((RI2(I)-RI1(I))**2+(ZI2(I)-ZI1(I))**2)
      IF(I.GT.NIN) CAPOUT=CAPOUT+CHAR*EPS3
      IF(I.LE.NIN) CAPIN=CAPIN+CHAR*EPS2
    5 CONTINUE
C
      CAPOUT=CAPOUT*2.0D0*3.1415926535D0
      CAPIN=CAPIN*2.0D0*3.1415926535D0
      CAP=CAPIN+CAPOUT
      WRITE(6,122)
      WRITE(6,123)
  123 FORMAT(1X,'CAPACITANCES NORMLZD TO FREE SPACE PERM AND PI :')
      WRITE(6,124)
  124 FORMAT(8X,'INSIDE',12X,'OUTSIDE',12X,'TOTAL')
      WRITE(6,125) CAPIN,CAPOUT,CAP
  125 FORMAT(1X,3D18.7)
  122 FORMAT(1X,' ')
C
C     CALCULATION OF NET FRINGING CAPACITANCE:
      CTEM=2.0D0*3.1415926535D0*2.05D0*4.0D0/(DLOG(3.268D0))
      CNORM=(CAP-CTEM)/2.268D0
      WRITE(6,122)
      WRITE(6,133)CTEM
  133 FORMAT(1X,'C-TEM',D20.9)
      WRITE(6,122)
      WRITE(6,130)
  130 FORMAT(1X,'NET FRINGING CAPACITANCE NORMALIZED TO FREE SPACE
     &PERMITTIVITY AND (B-A):')
      WRITE(6,131)CNORM
  131 FORMAT(1X,'   C/EPS*(B-A) = ',D17.7)
C
      STOP
      END
C
```

```
C     SUBROUTINE SECTION
C     ------------------
C
      SUBROUTINE GAUSS(RI,ZI,RJM,RJP,ZJM,ZJP,S,KCODE)
C     ..................................................
C     SINGLE INTEGRATION SUBROUTINE: UTILIZES VARIABLE-POINT
C     LEGENDRE-GAUSS QUADRATURE APPLIED TO A SINGLE INTEGRAL.
C     ..................................................
      IMPLICIT REAL*8 (A-H,O-Z)
      REAL*8 F(16),U4(4),H4(4),U6(6),H6(6),U8(8),H8(8),
     &U10(10),H10(10),U16(16),H16(16)
C     NIP IS THE NO. OF INTEGRATION POINTS:
      COMMON/GAUSS1/U4,H4,U6,H6,U8,H8,U16,H16
      COMMON/GAUSS2/U10,H10
      NIP=16
C     CALCULATE THE KERNEL FUNCTION:
      DO 1 I=1,NIP
      RJ=((RJP+RJM)+U16(I)*(RJP-RJM))/2.0D0
      ZJ=((ZJP+ZJM)+U16(I)*(ZJP-ZJM))/2.0D0
      CALL DERIV(RI,ZI,RJ,ZJ,FF,KCODE)
      F(I)=FF*RJ
    1 CONTINUE
C     CONSTRUCT THE INTEGRAL
      S=0.0D0
      DO 2 I=1,NIP
      S=S+H16(I)*F(I)
    2 CONTINUE
      S=S*DSQRT((RJP-RJM)**2+(ZJP-ZJM)**2)/2.0D0
      RETURN
      END
C
C
C
C
      SUBROUTINE DIRZ(RI,ZI,RJ,Z1,Z2,SUM)
C     ..................................................
C     DIRECT INTEGRATION OF THE REGULAR GREEN'S FUNCTION
C     USING GUASS-CHEBYCHEF QUADRATURE
C     ..................................................
      IMPLICIT REAL*8 (A-H,O-Z)
      F(X)=DLOG(DABS(((ZI-Z2)+DSQRT((RI+RJ)**2-4.D0*RI*RJ*X*X
     &+(ZI-Z2)**2))/((ZI-Z1)+DSQRT((RI+RJ)**2-4.D0*RI*RJ*X*X
     &+(ZI-Z1)**2))))
C     N-NUMBER OF INTEGRATION STEPS
      N=1000
      YN=N
      SUM=0.0D0
      DO 1 I=1,N
      YI=I
      X=DCOS((2.0D0*YI-1.D0)*3.1415926535898D0/(4.D0*YN))
      SUM=SUM+DABS(F(X))
    1 CONTINUE
      SUM=SUM*RJ/(2.0D0*YN)
      RETURN
      END
```

```
C
      SUBROUTINE GREEN(R1,Z1,R2,Z2,G)
C     This routine calculate the Green's function
C     ..................................................
      IMPLICIT REAL*8 (A-H,O-Z)
      REAL*8 MMDELK,ARG,G
      IOPT=1
C     ARG IS THE ARGUMENT OF THE ELLIPTIC INTEGRAL OF 1ST KIND
      ARG=4.0D0*R1*R2/((R1+R2)**2+(Z1-Z2)**2)
C     MMDELK - IBM-IMSL elliptic integral subroutine
      H=MMDELK(IOPT,ARG,IER)
      G=H/DSQRT((R1+R2)**2+(Z1-Z2)**2)
      G=G/3.14159265358979D0
      RETURN
      END
C
      SUBROUTINE DERIV(R,Z,RP,ZP,DG,DCODE)
C
C     ..................................................
C     This routine calculates the derivatives of the
C     Green's function w.r.t. r-axis or z-axis according
C     to the value of the DCODE.
C     DCODE=1   REGULAR GREEN'S FUNCTION
C     DCODE=2   DERIVATIVE W.R.T. Z-AXIS
C     DCODE=3   DERIVATIVE W.R.T. R-AXIS
C     ..................................................
      IMPLICIT REAL*8 (A-H,O-Z)
      REAL*8 DG,RP,ZP,R2,Z2
      INTEGER DCODE
C     DELTA - Finite difference step size
      DELTA=1.0D-7
      IF(DCODE.EQ.1) GOTO 5
      IF(DCODE.EQ.2) GOTO 2
C
C     Derivative w.r.t. R-axis
      CALL GREEN(R,Z,RP,ZP,G1)
      R2=R-DELTA*DABS(R)
      CALL GREEN(R2,Z,RP,ZP,G2)
      DG=(G1-G2)/(DELTA*DABS(R))
      RETURN
C
C     Derivative w.r.t. Z-axis
    2 CALL GREEN(R,Z,RP,ZP,G1)
      Z2=Z-DELTA*DABS(Z)
      CALL GREEN(R,Z2,RP,ZP,G2)
      DG=(G1-G2)/(DELTA*DABS(Z))
      RETURN
C
C     Regular Green's function
    5 CALL GREEN(R,Z,RP,ZP,G3)
      DG=G3
      RETURN
      END
```

```
C
C
      BLOCK DATA
C     ----------
C     ..................................................
C     Data block containing Gaussian quadrature
C     weights and abscissae.
C     U,V - abscissae
C     H,M - weights
C     ..................................................
      REAL*8 U4(4),H4(4),U6(6),H6(6),U8(8),H8(8),U10(10),H10(10),
     &U16(16),H16(16),V5(5),M5(5),V9(9),M9(9)
C
      COMMON/GAUSS1/U4,H4,U6,H6,U8,H8,U16,H16
      COMMON/GAUSS2/U10,H10
      COMMON/GAUSS3/V9,M9,V5,M5
      DATA U4/-.8611363115941D0,-.3399810435849D0,
     &.3399810435849D0,.8611363115941D0/
C
      DATA H4/.3478548451375D0,.6521451548625D0,
     &.6521451548625D0,.3478548451375D0/
C
      DATA U6/-.932469514 2D0,
     &-.6612093865D0,-.238619186 1D0,
     &.238619186 1D0,.6612093865D0,.932469514 2D0/
C
      DATA H6/.1713244924D0,
     &.3607615730D0,.4679139346D0,
     &.4679139346D0,.3607615730D0,.1713244924D0/
C
      DATA U8/-.1834346424957D0,-.5255324099163D0,
     &-.7966664774136D0,-.9602898564975D0,.9602898564975D0,
     &.7966664774136D0,.5255324099163D0,.1834346424957D0/
C
      DATA H8/.3626837833784D0,.3137066458779D0,
     &.2223810344534D0,.1012285362904D0,.1012285362904D0,
     &.2223810344534D0,.3137066458779D0,.3626837833784D0/
C
      DATA U10/-.1488743389816D0,
     &-.4333953941292D0,-.6794095682990D0,
     &-.8650633666890D0,-.9739065285172D0,.9739065285172D0,
     &.8650633666890D0,.6794095682990D0,.4333953941292D0,
     &.1488743389816D0/
C
      DATA H10/.2955242247147 5D0,
     &.2692667193 10D0,.2190863625 16D0,
     &.1494513491506D0,.0666713443087D0,.0666713443087D0,
     &.1494513491506D0,.2190863625 16D0,.2692667193 10D0,
     &.2955242247147 5D0/
C
```

```
      DATA U16/-.9894009349916D0,-.9445750230732D0,
     &-.8656312023878D0,-.7554044083550D0,-.6178762444026D0,
     &-.4580167776572D0,-.2816035507793D0,-.0950125098376D0,
     &.0950125098376D0,.2816035507793D0,.4580167776572D0,
     &.6178762444026D0,.7554044083550D0,.8656312023878D0,
     &.9445750230732D0,.9894009349916D0/
C
      DATA H16/.0271524594118D0,.0622535239386D0,
     &.0951585116825D0,.1246289712555D0,.1495959888166D0,
     &.1691565193950D0,.1826034150449D0,.1894506104551D0,
     &.1894506104551D0,.1826034150449D0,.1691565193950D0,
     &.1495959888166D0,.1246289712555D0,.0951585116825D0,
     &.0622535239386D0,.0271524594118D0/
C
      DATA V5/-.9061798459D0,-.5384693101D0,0.0D0,
     &.5384693101D0,.9061798459D0/
C
      DATA M5/.2369268851D0,.4786286705D0,.5688888889D0,
     &.4786286705D0,.2369268851D0/
C
      DATA V9/-.9681602395076D0,-.8360311073266D0,
     &-.6133714327006D0,-.3242534234038D0,0.0D0,
     &.3242534234038D0,.6133714327006,.8360311073266,
     &.9681602395076D0/
C
      DATA M9/.0812743883616D0,.1806481606949D0,
     &.2606106964029D0,.3123470770400,.3302393550013D0,
     &.3123470770400,.2606106964029D0,.1806481606949D0,
     &.0812743883616D0/
      END
```

A.2 SUBROUTINE GREEN OF THE METHOD OF IMAGES

```
C     ***************************************************
C     *  PROGRAM NAME: IMAGE FORTRAN                    *
C     *                                                 *
C     *  SUBROUTINE OF THE GREEN'S FUNCTION.            *
C     ***************************************************
      SUBROUTINE GREEN(R1,Z1,R2,Z2,G)
C     .................................................
      IMPLICIT REAL*8 (A-H,O-Z)
      REAL*8 MMDELK,ARG,G,G1,G2(60),ARG3(60),ARG5(60),B(60),
     &C(60),ALPHA(60),BETA(60),G3(60),G4(60),GN,DN
C
C     A = Displacement of the air wall from the origin.
      A=6.0D0
C     REFL is the image coefficient of water medium
C          backed by air wall.
      REFL=79.0D0/81.0D0
      IOPT=1
C     MMDELK is the IBM-IMSL elliptic integral subroutine.
C     ARG is the argument of the elliptic integral of first kind.
      ARG=4.0D0*R1*R2/((R1+R2)**2+(Z1-Z2)**2)
      H=MMDELK(IOPT,ARG,IER)
      G1=H/DSQRT((R1+R2)**2+(Z1-Z2)**2)
C
C     NTERM is the number of terms of the convergent series.
      NTERM=2
      DO 3 N=1,NTERM
      DN=DFLOAT(N)
      ALPHA(N)=(R1+R2)**2+(Z1-(2*DN*A)+((-1.0D0)**(N+1))*Z2)**2
      BETA(N)=(R1+R2)**2+(Z1+(2*DN*A)+((-1.0D0)**(N+1))*Z2)**2
      ARG3(N)=4.0D0*R1*R2/ALPHA(N)
      ARG5(N)=4.0D0*R1*R2/BETA(N)
      B(N)=MMDELK(IOPT,ARG3(N),IER)
      C(N)=MMDELK(IOPT,ARG5(N),IER)
      G2(N)=(REFL**N)*B(N)/DSQRT(ALPHA(N))
      G3(N)=(REFL**N)*C(N)/DSQRT(BETA(N))
      G4(N)=G2(N)+G3(N)
C
C
    3 CONTINUE
C
      GN=0.0D0
      DO 4 N=1,NTERM
    4 GN=GN+G4(N)
      G=G1+GN
      G=G/3.14159265358979D0
      RETURN
      END
```

Appendix B

COMPUTER PROGRAM FOR THE MEASUREMENTS

The computer program for the measurement system using a 6.4-mm open-ended coaxial line sensor and the Automated Network Analyzer was written in HP language (HPL) and can be executed on the HP9825A Desktop Computer.

```
0: "DIELECTRIC PROPERTIES MEASUREMENT WITH HP8410B NETWORK ANALYSER";
1: "(PHASE LOOP LOCKED WITH HP8709A SYNCHRONIZER)";
2: "MODIFIED TO PRINT GAMMA ";
3:
4: "OPEN-ENDED COAXIAL PROBE CALIBRATED WITH TWO LIQUIDS";
5:
6: "INITIALIZATION AND FREQUENCY ENTRY";
7: 0→r11
8: dim Q$[6,5],T$[4,4],C[40],X$[80],D[5,40],F[6],P$[1],P[40],R[40]
9: dim S[4,80],E[3,80],W[80],K[12],X[80],G[80],O[2],H[40],L[40],I[2],M$[80]
10: dim T[20],B[80],A[6],J[10]
11: .3239→K[2];.3779→K[3];50→K[4];1.9526→K[6];.0404→K[7];8.854→K[8]
12: 3→Q;20.278→r21;1→r20
13: "A46B5"→Q$[6,1];"A6B45"→Q$[5,1];"A45B6"→Q$[4,1]
14: "A5B46"→Q$[3,1];"A4B56"→Q$[2,1];"B456"→Q$[1,1]
15: "B23"→T$[1,1];"A2B3"→T$[2,1];"A3B2"→T$[3,1];"A23"→T$[4,1]
16: ent "Record Data ? Y/N",P$;if car(P$)="Y";1→r10
17: if r10=1;dsp "Insert Formatted Cassette";beep;stp
18: if r10=1;trk 0;rew
19: "Freq":ent "BAND? LOW(1) MED(2) HIGH(3)",A
20: if A=1;10→r1;2390→r2;10000/2390→r4;1→r18;sto +3
21: if A=2;1987→r1;8387→r2;10000/6400→r4;0→r18;sto +2
22: if A=3;5900→r1;12400→r2;10000/6500→r4;0→r18
23: lcl 7;rem 7
24: ent "PROBE DIAM.?:.141in(1),.250in(2)",A
25: if A=1;.0217→K[1];1.034→K[5];.63→K[9]
26: if A=2;.0388→K[1];1.848→K[5];3.6→K[9]
27: "FREQS":ent "START FREQ.(MHZ)",F[1]
28: ent "STOP FREQ.(MHZ)",F[2]
29: ent "FREQ.STEP (MHZ)",F[3]
30: int((F[2]-F[1])/F[3])+1→F[4]
31: if F[4]>40;sto "FREQS"
32: dsp "SET TEST CHANNEL GAIN TO 60 DB";stp
33: 0→O;6→Q;wrt 716,Q$[6,1]
34: (F[1]-r1)r4→F[6]
35: fmt 1,"M1V",f4.0,"E";wrt 706.1,F[6]-(F[6]>9999.5);wait 50
36: F[1]+r21→r22;r22/(int(r22/140)+1)→r22
37: if r20=1;wrt 707,"AP13DMFR",r22,"MZ";wait 75
```

```
38: beep;dsp "PRESS AND HOLD BEAM CENTRE ";stp
39: wrt 705,"H1AJ"
40: rot(rdb(705),8)+rdb(705)>D[1];.0025*D[1]>D[1]
41: wrt 705,"H2AJ"
42: rot(rdb(705),8)+rdb(705)>D[2];.0025*D[2]>D[2]
43: dsp "RELEASE BEAM CENTRE ";stp
44: sto "CAL"
45:
46:
47: "CALIBRATION SECTION":
48: "CAL":beep;dsp "END OF PROBE OPEN";stp
49: 0>O;6>Q;wrt 716,Q$[6,1]
50: 3>M
51: for N=1 to F[4]
52: ssb "READ"
53: next N
54: beep;dsp "IMMERSE PROBE IN WATER";stp
55: 0>O;6>Q;wrt 716,Q$[6,1]
56: 2>M
57: for N=1 to F[4]
58: ssb "READ"
59: next N
60: ssb "WATER"
61: if r18=1;beep;dsp "IMMERSE PROBE IN SALINE WATER";stp
62: if r18=0;beep;dsp "IMMERSE PROBE IN METHANOL ";stp
63: 0>O;6>Q;wrt 716,Q$[6,1]
64: 1>M
65: for N=1 to F[4]
66: ssb "READ"
67: next N
68: if r18=1;ssb "SALINE"
69: if r18=0;ssb "METHAN"
70: ssb "CALREF"
71:
72: "MEAS":beep
73: ent "SET-UP MEASURE, ENTER LABEL",X$
74: 4>M
```

```
75: for N=1 to F[4]
76: gsb "READ"
77: next N
78: gsb "MESREF"
79: fxd 0;wrt 11,r11
80: wrt 11,X$
81: if r18=1;wrt 11,"CALIBRATED WITH OPEN,SALINE AND WATER "
82: if r18=0;wrt 11,"CALIBRATED WITH OPEN,METHANOL AND WATER"
83: fmt 2,"MHz",9x,"E1",6x,"E2",7x,"TAN   SE(mS/cm)  MAG",5x,"ANG",z;wrt 11,2
84: wrt 11,"     Ct(pf)"
85: sto "OUT"
86:
87: "SUBROUTINE SECTION":
88:
89: "READ":(F[1]+(N-1)F[3]-r1)r4>F[6]
90: fmt 1,"M1V",f4.0,"E"
91: wrt 706.1,F[6]-(F[6]>9999.5);wait 75
92: F[1]+(N-1)F[3]>r23;r23+r21>r22;r22/(int(r22/140)+1)>r22
93: fxd 6
94: if r20=1;wrt 707,"AP13DMFR",r22,"MZ";wait 200
95: fxd 2;dsp "CURRENT FREQ. ",r23," MHz"
96: if N=1;wait 500
97: 8>Z;gsb "VOLT"
98: if V<-2.5;sto "MARK"
99: dsp "NO PHASE-LOCK";beep;stp
100: sto "READ"
101: "MARK":1>Z;gsb "VOLT"
102: V-O[1]>E;2>Z;gsb "VOLT"
103: cll 'R/P'(E,V-O[2],B,A)
104: if B>2.2;sto "UP"
105: if B<.4;sto "DWN"
106: "SCA":4>Z;gsb "VOLT"
107: tn^(2V)>B;cll 'P/R'(B,A,X,Y)
108: X>S[M,N];Y>S[M,N+40]
109: ret
110:
```

```
111: "UP":Q+1→Q;if Q>6;6→Q;prt "OVER RANGE";sto "SCA"
112: sto "ATTEN"
113: "DWN":Q-1→Q;if Q<1;1→Q;sto "SCA"
114: "ATTEN":wrt 716,Q$[Q,1];wait 500
115: sto "READ"
116:
117: "VOLT":0→W;2+(Q=1)8+(Q=2)4→D;for L=1 to D
118: fmt 1,"H",f.0,"AJ";wrt 705.1,Z
119: if N=1;wait 500
120: rot(rdb(705),8)+rdb(705)→V
121: W+V→W;next L;W/D→V
122: .0025V→V;ret
123:
124: "CALREF":for N=1 to F[4]
125: S[1,N]-S[2,N]→T[1];S[1,N+40]-S[2,N+40]→T[2]
126: S[3,N]-S[1,N]→T[3];S[3,N+40]-S[1,N+40]→T[4]
127: S[2,N]-S[3,N]→T[5];S[2,N+40]-S[3,N+40]→T[6]
128: F[1]+(N-1)F[3]→F[5]
129: K[1]+K[9]F[5]*F[5]*1e-11→K[10]
130: cll 'P/R'(1,-atn(2(F[5]K[10]K[4]2e-6),T[7],T[8])
131: cll 'C*'(G[N],G[N+40],B[N],B[N+40],T[9],T[10])
132: cll 'C*'(B[N],B[N+40],T[7],T[8],T[11],T[12])
133: cll 'C*'(G[N],G[N+40],T[7],T[8],T[13],T[14])
134: cll 'C*'(T[9],T[10],T[1],T[2],T[15],T[16])
135: cll 'C*'(T[11],T[12],T[3],T[4],T[17],T[18])
136: cll 'C*'(T[13],T[14],T[5],T[6],T[19],T[20])
137: T[15]+T[17]+T[19]→T[1];T[16]+T[18]+T[20]→T[2]
138: cll 'C*'(S[3,N],S[3,N+40],T[15],T[16],T[3],T[4])
139: cll 'C*'(S[1,N],S[1,N+40],T[19],T[20],T[7],T[8])
140: cll 'C*'(S[2,N],S[2,N+40],T[17],T[18],T[5],T[6])
141: T[3]+T[7]+T[5]→T[11];T[4]+T[8]+T[6]→T[12]
142: cll 'C/'(T[11],T[12],T[1],T[2],E[1,N],E[1,N+40])
143: S[2,N]-E[1,N]→T[1];S[2,N+40]-E[1,N+40]→T[2]
144: S[1,N]-E[1,N]→T[3];S[1,N+40]-E[1,N+40]→T[4]
145: cll 'C*'(B[N],B[N+40],T[1],T[2],T[5],T[6])
146: cll 'C*'(G[N],G[N+40],T[3],T[4],T[7],T[8])
147: cll 'C/'(T[7]-T[5],T[8]-T[6],T[15],T[16],E[2,N],E[2,N+40])
148: cll 'C*'(E[2,N],E[2,N+40],B[N],B[N+40],T[1],T[2])
149: cll 'C*'(1-T[1],-T[2],T[3],T[4],T[5],T[6])
150: cll 'C/'(T[5],T[6],B[N],B[N+40],E[3,N],E[3,N+40])
```

```
151: next N
152: ret
153:
154: "MESREF":for N=1 to F[4]
155: S[4,N]-E[1,N]→T[3];S[4,N+40]-E[1,N+40]→T[4]
156: cll 'C//'(T[3],T[4],E[3,N],E[3,N+40],T[1],T[2])
157: cll 'C*'(T[1],T[2],E[2,N],E[2,N+40],T[3],T[4])
158: 1+T[3]→T[3]
159: cll 'C//'(T[1],T[2],T[3],T[4],X[N],X[N+40])
160: next N
161: ret
162:
163: "P/R":P1cos(P2)→P3
164: P1sin(P2)→P4
165: ret
166: "R/P":√(P1P1+P2P2)→P3
167: 90(sgn(P2)+(P2=0))→P4
168: If P1=0;sto +2
169: atn(P2/P1)+P4(1-sgn(P1))→P4
170: ret
171: "C/":P3P3+P4P4→P7
172: (P1P3+P2P4)/P7→P5
173: (P2P3-P1P4)/P7→P6
174: ret
175: "C*":P1P3-P2P4→P5
176: P1P4+P2P3→P6
177: ret
178:
179: "OUTPUT DATA SECTION":
180: "OUT":0→r7;0→r8;0→r9;0→r12;0→r13;0→r14;0→r15;0→r16
181: for N=1 to F[4]
182: cll 'R/P'(X[N],X[N+40],T[1],T[2])
183: F[1]+(N-1)F[3]→C[N]
184: K[1]+K[9]C[N]*C[N]*1e-11→K[10]
185: (1+2*T[1]*cos(T[2])+T[1]*T[1])*2*(*C[N]*K[4]*K[10]/1000000)→R
186: 2*T[1]*sin(-T[2])/R→U
```

```
187: K[7]+K[3](UK[2]/(1+UK[2]))→K[11];K[5]K[8]K[11]1e-3→K[12]
188: K[12]/(K[10]-K[12])→S
189: 2*T[1]*(1+S)*sin(-T[2])/R-S→U
190: (1-T[1]*T[1])(1+S)/R→L
191: L/U→T;L*2*(*K[8]*C[N]*1e-5→B
192: 2(C[N]1e-6*50(1+2T[1]cos(-T[2])+T[1]T[1]))→J[1]
193: (1-T[1]T[1])/LJ[1]→J[2]
194: 2T[1]sin(-T[2])/J[1]-UJ[2]→J[3]
195: \(UU+LL)→J[4]
196: J[3]+J[4]J[2]→J[5]
197: fmt 3,f7.1,2x,f6.2,2x,f7.2,2x,f7.3,2x,f7.2,2x,f6.2,2x,f6.1,2x,f6.4
198: C[N]→D[1,N];U→D[2,N];L→D[3,N];T→D[4,N];B→D[5,N]
199: wrt 11.3,C[N],U,L,T,B,T[1],T[2],J[5]
200: next N
201: fmt 4,7/;wrt 11.4
202: if r10=1;rcf r11,X$,D[*],F[*]
203: r11+1→r11
204: if r11>99;dsp "TAPE IS FULL";stp
205: beep;ent "(C)alibrate or (M)easure ?",P$
206: if cap(P$)="C";sto "Freq"
207: sto "MEAS"
208:
209: "CALCULATION OF LIQUIDS PERMITTIVITY":
210: "METHAN":beep;ent "TEMPERATURE OF METHANOL ?",T
211: 4.45→E;39.2-.22*T→P;.036→Z
212: T+273.15→T
213: 886/T-2.28→K;20(10^K→G
214: G*1e-6→G
215: gsb "COLE"
216: ret
217:
218: "WATER":beep;ent "TEMPERATURE OF WATER ?",T
219: 4.6→E;.014→Z
220: .40008*T→G;.0009398*T*T→H;.00000141*T*T*T→R
221: 87.74-G+H-R→P
```

```
222: 3.824*T→G;.06938*T*T→H;.0005096*T*T*T→R
223: 111.09-G+H-R→G
224: G*1e-6→G
225: ssb "COLE"
226: ret
227:
228: "COLE":for N=1 to F[4]
229: F[1]+(N-1)F[3]→F[5]
230: K[1]+K[9]F[5]F[5]1e-11→K[10]
231: G*F[5]→W;(1-Z)*ln(W)→W;exp(-W)→A[2];exp(W)+exp(-W)→A[1]
232: sin(-Z/2)→A[3];cos(-Z/2)→A[4]
233: (P-E)(A[2]+A[3])/(A[1]+2A[3])+E→A
234: (P-E)A[4]/(A[1]+2A[3])→B
235: K[7]+K[3](AK[2]/(1+AK[2]))→K[11];K[5]K[8]K[11]*1e-3→K[12]
236: 2-(F[5]K[4]K[10]*1e-6→K
237: 2-(F[5]K[4]K[12]*1e-6→I
238: cll 'C*'(0,K-I,A,-B,C,D)
239: cll 'C/'(1-C,-(D+1),1+C,D+1,X,Y)
240: if M=1;X→B[N];Y→B[N+40]
241: if M=2;X→G[N];Y→G[N+40]
242: fmt 8,f4.1,x,f5.2,x,f5.2
243: fmt 9,"GHz    E1    E2"
244: if N=1;wrt 16,9
245: F[5]/1000→F[5]
246: wrt 16.8,F[5],A,B
247: next N
248: ret
249:
250: "CALCULATION OF SALINE WATER PERMITTIVITY":
251: "SALINE":beep;ent "TEMPERATURE OF SALINE SOL'N ?",T
252: beep;ent "SALINITY in ppt ?",S
253: .01707*S+1.205*S*S*1e-5+4.058*S*S*S*1e-9→V
254: 4.6→E
255: .40008*T→G;9.398*T*T*1e-4→H;1.41*T*T*T*1e-6→I
256: 87.74-G+H-I→F
257: .2551*V→G;.05151*V*V→H;6.889*V*V*V*1e-3→I
```

```
258: 1-G+H-I)A;F*A)A
259: 3.824*T)G;.06938*T*T)H;5.096*T*T*T*1e-4)R
260: 111.09-G+H-R)Z;Z/1000)Z
261: .001463*V*T)G;.04896*V)H;.02967*V*V)I;.005644*V*V*V)J
262: 1+G-H-I+J)U;U*Z)L
263: 25-T)D
264: 10.394*V)G;2.3776*V*V)H;.68258*V*V*V)I
265: .13538*V^4)J;.010086*V^5)K
266: G-H+I-J+K)R
267: 3.02*D*V*1e-5)G;3.922*D*D*V*1e-5)H;1.721*D*V*V*1e-5)I
268: 6.584*D*D*V*V*1e-6)J
269: G+H+I-J)K
270: .01962*D)G;8.08*D*D*1e-5)H
271: R*(1-G+H-K))J
272: for N=1 to F[4]
273: if r6=0;F[1]+(N-1)F[3])C[N]
274: L*C[N])W;W/1000)W;1+W*W)H
275: (A-E)/H)B;B+E)I[1]
276: 2(*K[8]*C[N]1e-6)I
277: B*W+J/I)I[2]
278: K[1]+K[9]*C[N]*C[N]*1e-11)K[10]
279: K[7]+K[3](I[1]K[2]/(1+I[1]K[2])))K[11];K[5]K[8]K[11]*1e-3)K[12]
280: 2(C[N]K[10]K[4]*1e-6)K
281: 2(C[N]K[4]K[12]*1e-6)I
282: cll 'C*'(0,K-I,I[1],-I[2],C,D)
283: cll 'C/'(1-C,-(D+I),1+C,D+I,X,Y)
284: X)B[N];Y)B[N+40]
285: fmt 9,f4.0,x,f5.2,x,f6.1
286: wrt 16.9,C[N],I[1],I[2]
287: next N
288: ret
289: end
*12477
```

Example of data printout

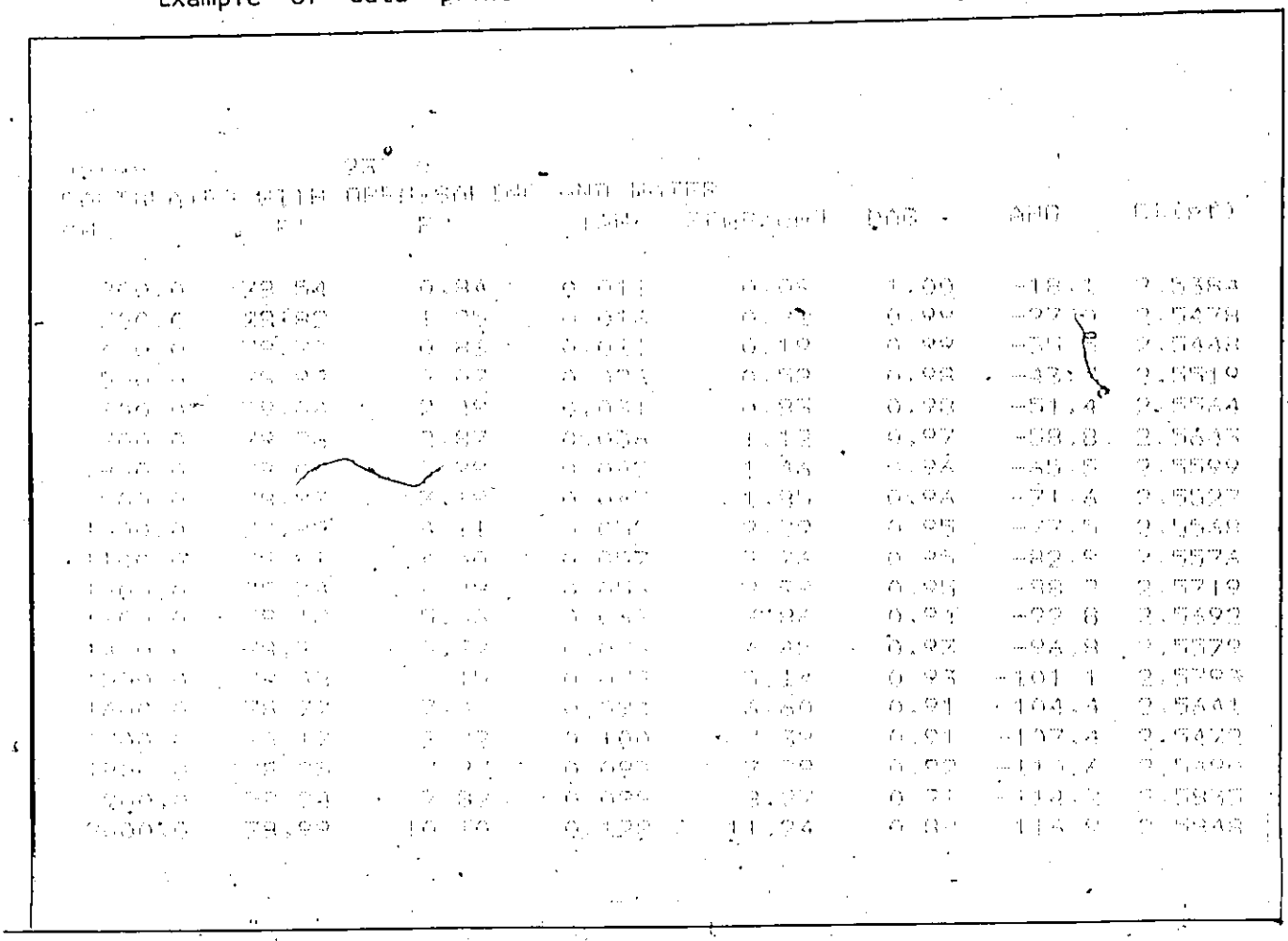

BIBLIOGRAPHY

1. Stuchly, M. A. Interaction of Radio Frequency and Microwave Radiation with Living Systems. Rad. and Environm. Biophys. vol.16, pp. 1-14. 1979.

2. Schwan, H.P., Foster, K.R. RF-Field Interactions with Biological Systems: Electrical Properties and Biophysical Mechanisms. Proc. IEEE, vol. 68, pp. 104-113, 1980.

3. Durney, C.H. Electromagnetic Dosimetry for Models of Humans And animals: A Review of Theoretical and Numerical Techniques. Proc. IEEE, vol.68, no.1, pp.33-40, Jan.1980.

4. Michaelson, S.M. Human Exposure to Non-Ionizing Radiant Energy Potential Hazards and Safety Standards. Proc. IEEE, vol. 60, pp. 389-421, 1974.

5. Christensen, D.A., Durney, C.H. Hyperthermia Production for Cancer Therapy: A Review of Fundamentals and Methods. J.Microwave Power, vol.16, no.2., pp. 89-105, Jun.1981.

6. Ecker, H. A., Burdette, E. C., Cain, F. L. Simultaneous Microwave and High Frequency Thawing of Cryogenically Preserved canine kidneys. IEEE Int. Symp. Electromagn. Compat., pp. 226-230, July 1976.

7. Schepps, J.L., Foster, K.R. UHF and Microwave Dielectric Properties of Normal and Tumor Tissues: Variation in Dielectric Properties with Tissues Water Content. Phys. Med. Biol., vol.25, pp. 1149-1159, 1980.

8. Stuchly, M. A., Stuchly, S. S. Dielectric Properties of Biological Substances--Tabulated. Journal of Microwave Power., vol. 15, no. 1., 1980. pp. 19-26.

9. Stoy, R. D., Foster, K. R., Schwan, H. P. Dielectric Properties of Mammalian Tissues from 0.1 to 100 MHz: A Summary of Recent Data. Phys. Med. Biol., vol. 27, no. 4, pp. 501-513. 1982.

10. Athey, T. W., Stuchly, M. A., Stuchly, S. S. Measurement of Radio Frequency Permittivity of Biological Tissues with an Open-Ended Coaxial Line: Part 1. IEEE Trans. Microwave Theory and Techniques, vol. MTT-30, no. 1, Jan. 1982.

11. Stuchly, M. A., Athey, T. W., Samaras, G. M., Taylor, G. E. Measurement of Radio Frequency Permittivity of Biological Tissues with an Open-Ended Coaxial Line: Part 2--Experimental Results. IEEE Trans. Microwave Theory and Techniques, vol. MTT-30, no. 1, Jan. 1982.

12. Kraszewski, A., Stuchly, M. A., Stuchly, S. S., Smith, A. M. In Vivo and In Vitro Dielectric Properties of Animal Tissues at Radio Frequencies. Bioelectromagnetics, vol 3, 1982. pp. 421-432.

13. Brady, M. M., Symons,S. A., Stuchly, S. S. Dielectric Behaviour of Selected Animal Tissues in vitro at Frequencies from 2 to 4 GHz. IEEE Trans. Biomed. Eng., vol. BME-28, no. 3, March 1981. pp. 305-307.

14. Bussey, H. E. Measurement of RF Properties of Materials A Survey. Proc. IEEE., vol. 55, no. 6, pp. 1046-1053, June 1967.

15. Alschuler, L. Dielectric Constant. in Handbook of Microwave Measurements, vol. 3, M.Sucher and J.Fox, Eds.Brooklyn, NY : Polytechnic Press, Chapter 9, 1963.

16. Stuchly, S. S., Matuszewski, M. .A Combined Total Reflection-Transmission Method in Application in Dielectric Spectroscopy. IEEE Trans. Instrum. Meas., vol. IM-27, no. 3, Sept. 1978. pp. 285-288.

17. Von Hippel, A. R., Ed. Dielectric Materials and Applications. New York, NY., Wiley, 1954.

18. Stuchly, M. A., Stuchly, S. S. Coaxial Line Reflection Method for Measuring Dielectric Properties of Biological Substances at Radio and Microwave Frequencies-A Review. IEEE Trans. Instrum. Meas., vol. IM-29, no. 3, pp. 176-183. Sept 1980.

19. Tanabe, E., and Joines, W. T. A Nondestructive Method for Measuring the Complex Permittivity of Dielectric Materials at Microwave Frequencies Using an Open Transmission Line Resonator. IEEE Trans. Instrum. Meas., vol. IM-25, no. 3, pp. 222-226, Sept. 1976.

20. Iskander, M. F., Stuchly S. S., Fringing Field Effect in the Lumped-Capacitance Method for Permittivity Measurement. IEEE Trans. Instrum. Meas., vol. IM-27, no. 1, March 1978. pp. 107-109.

21. Rzepecka, M. A., Stuchly, S. S. A Lumped Capacitance Method for the Measurement of the Permittivity and Conductivity in the Frequency and Time Domain--A further Analysis. IEEE Trans. Instrum. Meas., vol. IM-24, no. 1, March, 1975. pp. 27-32.

22. Stuchly, S. S., Rzepecka, M. A., Iskander, M. F., Permittivity Measurements at Microwave Frequencies Using Lumped Elements. IEEE Trans. Instrum. Meas., vol. IM-23, no. 1, March 1974. pp. 56-62.

23. Burdette, E. C., Cain, F. L., Seals, J. In Vivo Probe Measurement Technique for Determining Dielectric Properties at VHF Through Microwave Frequencies. IEEE Trans. Microwave Theory Tech., vol. MTT-28, Apr. 1980. pp. 414-427.

24. Gajda, G. B. A Method for Measurement of Permittivity at Radio and Microwave Frequencies. IEEE Int. Electrical, Electronics Conf. and Exposition, Conf. Dig., Oct. 1979.

25. Mosig, J.R., Besson, J.E., Gex-Fabry, M., Gardiol, F.E. Reflection of an Open-Ended Coaxial Line and Application to Nondestructive Measurement of Materials. IEEE Trans. Instrum. Meas., vol. IM-30, no. 1, March 1981, pp. 46-50.

26. Stuchly, M. A., Brady, M. M., Stuchly S. S., Gajda, G. B. Equivalent Circuit of an Open-Ended Coaxial Line in a Lossy Dielectric. IEEE Trans. Instrum. Meas., vol. IM-31, no. 2, June 1982 pp. 116-119.

27. Gajda, G. B. and Stuchly, S. S. Numerical Analysis Of open-Ended Coaxial Lines. IEEE Trans. Microwave Theory Tech., vol. MTT-31, no. 5. May 1983, pp. 380-384.

28. Gajda, G. B. Numerical Analysis of in Vivo Dielectric Sensors. M.A.Sc. Thesis, University of Ottawa, Canada, Apr. 1982.

29. Harrington, R.F. Field Computation by Moment Methods. Macmillan, New York, 1968.

30. Silvester, P. TEM Wave Properties of Microstrip Transmission Lines. Proc. IEE, vol. 115, no. 1, Jan. 1968. pp. 43-48.

31. Daffe, J., Olsen, R. G. An Integral Equation Technique for solving Rotationally Symmetric Electrostatic Problems in Conducting and Dielectric Material. IEEE Trans. Power App. Sys., vol. PAS-98.,no. 5, Sept./Oct. 1979. pp. 1609-1616.

32. McDonald, B. H., Friedman, M., Wexler, A. Variational Solution of Integral Equations. IEEE Trans. Microwave Theory and Tech., vol. MTT-22, no. 3, March 1974. pp. 237-248.

33. IMSL Subroutine Library Reference Manual, 8 Edition, IMSL, Houston, Texas, June 1980.

34. Hewlett-Packard, Automating The HP 8410B Microwave Network Analyzer. Application Note 221A, Hewlett-Packard, June 1980.

35. Kraszewski, A., Stuchly, S.S. Capacitance of Open-ended Dielectric-filled Coaxial Lines -- Experimental Results. IEEE Trans. Instrum. Meas., vol. IM-32, no. 4, Dec. 1983, pp.517-519.

36. Kraszewski, A., Stuchly, S. S., Stuchly, M. A., Symons, S. A. On the Measurement Accuracy of the Tissue Permittivity In Vivo. IEEE Trans. Instrum. Meas., vol. IM-32, no. 1, March 1983, pp. 37-42.

37. Kraszewski, A. Guidelines for Measuring Permittivity Using Open-Ended Coaxial-Line Sensors and the HP8410B Automated Network Analyzer. Laboratory Application Note, University of Ottawa, April 1983.